Electronic Supplementary Material (ESI) for Organic Chemistry Frontiers.

Supporting Information

Fine-Tuning Macrocycle Cavity to Selectively Bind Guests in Water for Near-Infrared Photothermal Conversion

Fei Yang,[a] Yunong Li,[a] Ran Li,[b] Xiaolin Wang,[a] Xiangkun Cui,[b] Wei Wei[b] and Yanqing Xu[a]*

[a] Key Laboratory of Cluster Science, Ministry of Education of China, Beijing Key Laboratory of Photoelectronic/Electrophotonic Conversion Materials, School of Chemistry and Chemical Engineering, Beijing Institute of Technology, Beijing 100081, China. E-mail: xyq@bit.edu.cn

[b] Beijing Key Laboratory for Optical Materials and Photonic Devices, Department of Chemistry, Capital Normal University, Beijing 100048, P. R. China.

Table of Contents

1. Method and Synthesis

1.1 General Method.

All the reagents involved in this research were commercially available and used without further purification unless otherwise noted. Solvents were either employed as purchased or dried prior to use by standard laboratory procedures. ^{1}H and ^{13}C NMR spectra were recorded on a Bruker AVANCE III 600 spectrometer. All chemical shifts are reported in ppm with residual solvents or TMS (tetramethylsilane) as the internal standards. High-resolution electrospray-ionization mass spectrometry (HRMS) experiments were conducted on a Thermo Fisher Q Exactive mass spectrometer. UV-vis spectroscopy studies were performed on a Shimadzu UV-2550 spectrophotometer. 808 nm NIR laser (MDL-III-808-2.5W) was purchased from Changchun New Industries Optoelectronics Technology Co., Ltd. Thermal imaging was recorded by FOTRIC 326C camera.

1.2 Synthetic Routes of TBox-4^{2+}.

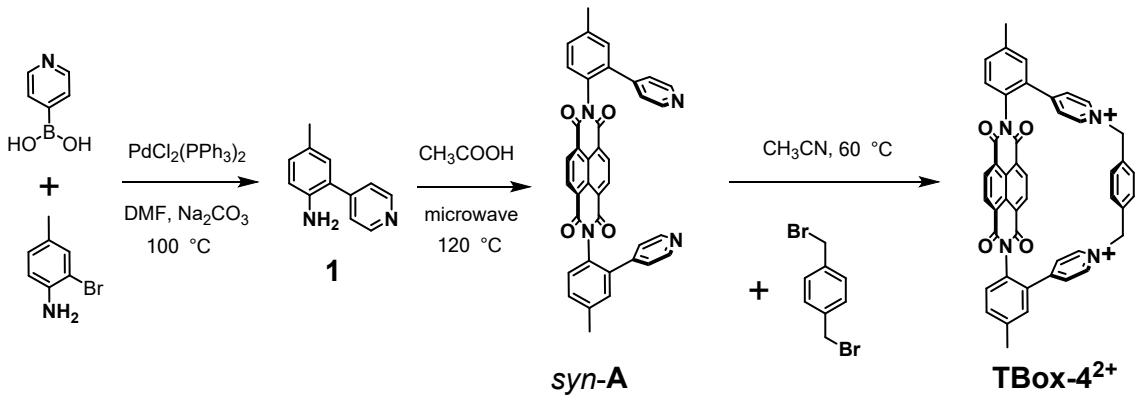

Synthesis of 1:

The solution of 2-bromo-4-methylaniline (1.861 g, 10 mmol) in DMF (30 mL) was degassed with nitrogen for 15 min followed by addition of Na_2CO_3 solution (20 mL, 2 M) under continuous flow of nitrogen. After 10 min, pyridine-4-boronic acid (1.476 g, 12 mmol) and $PdCl_2(PPh_3)_2$ (0.490 g, 0.7 mmol) were added to the reaction mixture under a nitrogen atmosphere. The reaction mixture was stirred at 100 °C for 5 h. The solution was diluted with H_2O (20 mL), and then the product was extracted three times with EtOAc (80 mL). The combined organic layer was dried over $MgSO_4$ and the solvent was removed in vacuo. The crude product was purified

on a silica gel column using petroleum ether/ethyl acetate (1:1, v/v) as eluent to afford the product as yellow solids (1.56 g, 85%). **1**: ^{1}H NMR (600 MHz, $CDCl_3$, 298 K): δ (ppm) = 8.666 (d, *J* = 4.8 Hz, 2H), 7.432 (d, *J* = 6.0 Hz, 2H), 7.026 (d, *J* = 7.8 Hz, 1H), 6.947 (s, 1H), 6.706 (d, *J* = 7.8 Hz, 1H), 2.284 (s, 3H); ^{13}C NMR (150 MHz, $CDCl_3$, 298 K): δ (ppm) = 150.20, 147.75, 140.81, 130.42, 130.32, 128.24, 124.45, 123.86, 116.27 (C of aromatic rings), 20.33 (C of methyl). HRMS (ESI) *m/z* calcd for [**1**+H]$^+$: 185.1079, found: 185.1072.

Synthesis of *syn*-A:

1,4,5,8-Naphthalenetetracarboxylic dianhydride (72 mg, 0.27 mmol) and **1** (124 mg, 0.675 mmol) were stirred in acetic acid (3 mL) under microwave irradiation (100 W, 30 min, 120 °C). After the solution was extracted three times with $CHCl_3$, the combined organic layer was dried over $MgSO_4$ and the solvent was removed in vacuo to give a brown solid. The crude product was purified on a silica gel column using petroleum ether/ethyl acetate (1:1, v/v) as eluent to afford the lower R_f *syn*-**A** as light yellow solids (64 mg, 40%). *syn*-**A**: ^{1}H NMR (600 MHz, DMSO-d_6, 298 K): δ (ppm) = 8.582 (s, 4H), 8.395 (d, *J* = 6.0 Hz, 4H), 7.480 (d, *J* = 8.4 Hz, 2H), 7.423 (d, *J* = 8.4 Hz, 2H), 7.352 (s, 2H), 7.171 (d, *J* = 6.0 Hz, 4H), 2.445 (s, 6H); ^{13}C NMR (150 MHz, $CDCl_3$, 298 K): δ (ppm) = 162.83, 149.75, 146.76, 140.06, 138.45, 131.39, 131.15, 130.63, 129.50, 128.84, 127.02, 126.47, 123.03 (C of aromatic rings), 21.29 (C of methyl). HRMS (ESI) *m/z* calcd for [*syn*-**A**+H]$^+$: 601.1876, found: 601.1863.

Synthesis of TBox-4^{2+}:

Syn-**A** (156 mg, 0.26 mmol) and p-xylylene dibromide (68 mg, 0.26 mmol) were stirred in dry CH_3CN at 60 °C for 4 h under nitrogen protection. The yellow precipitate was collected by vacuum filtration and dissolved in H_2O. When a satd aqueous solution of NH_4PF_6 was added to the reaction mixture, the resulting precipitate was filtered off and then washed with deionized H_2O. The precipitate was dried to afford pure **TBox-4**·2PF_6 (219 mg, 85%) as yellowish solids without further purification. **TBox-4**·2PF_6: ^{1}H NMR (600 MHz, DMSO-d_6, 298 K): δ (ppm) = 8.820 (d, *J* = 7.2 Hz, 4H), 8.597 (s, 4H), 7.984 (d, *J* = 6.6 Hz, 4H), 7.645 (s, 4H), 7.554 (s, 2H), 7.051 (s, 4H), 5.793 (s, 4H), 2.535 (s, 6H); **TBox-4**·2Br: ^{1}H NMR (600 MHz, D_2O, 298 K): δ (ppm) = 8.550 (s, 4H), 8.539 (s, 4H), 7.780 (d, *J* =7.2 Hz, 4H), 7.577 (d, *J* = 7.2 Hz, 2H), 7.537

(s, 2H), 7.399 (d, J = 8.4 Hz, 2H), 7.008 (s, 4H), 5.599 (s, 4H), 2.431 (s, 6H); ^{13}C NMR (150 MHz, DMSO-d_6, 298 K): δ (ppm) = 162.86, 155.94, 145.47, 140.15, 135.29, 135.19,132.51, 131.30, 130.49, 130.22, 130.04, 129.31, 127.77, 126.49,126.43 (C of phenyl and pyridyl), 62.57 (C of methylene), 21.19 (C of methyl). HRMS (ESI) *m/z* calcd for [**TBox-4**]$^{2+}$: 352.1207, found: 352.1200; *m/z* calcd for [**TBox-4**+PF_6]$^+$: 849.2060, found: 849.2037. Single crystals were grown by slow diffusion of ethyl acetate into an DMF solution of **TBox-4**·2PF_6 over 7 days.

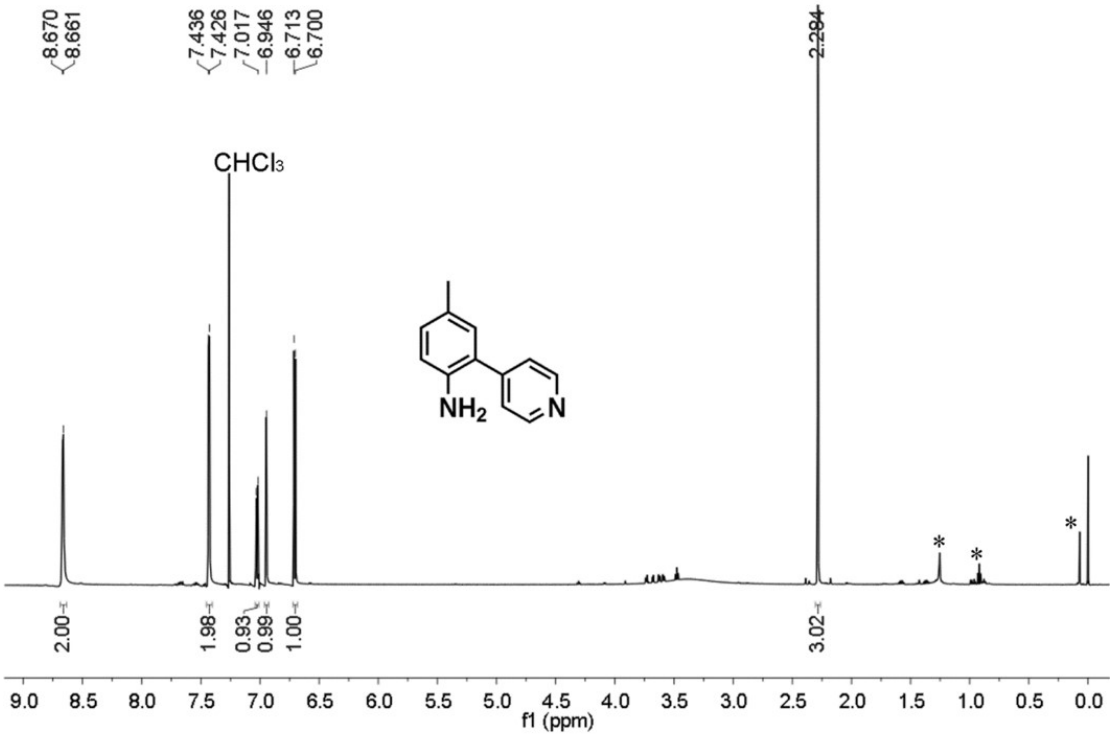

Fig. S1. ^{1}H NMR spectrum of **1** in $CDCl_3$. The signals of small amounts of impurities are marked with *.

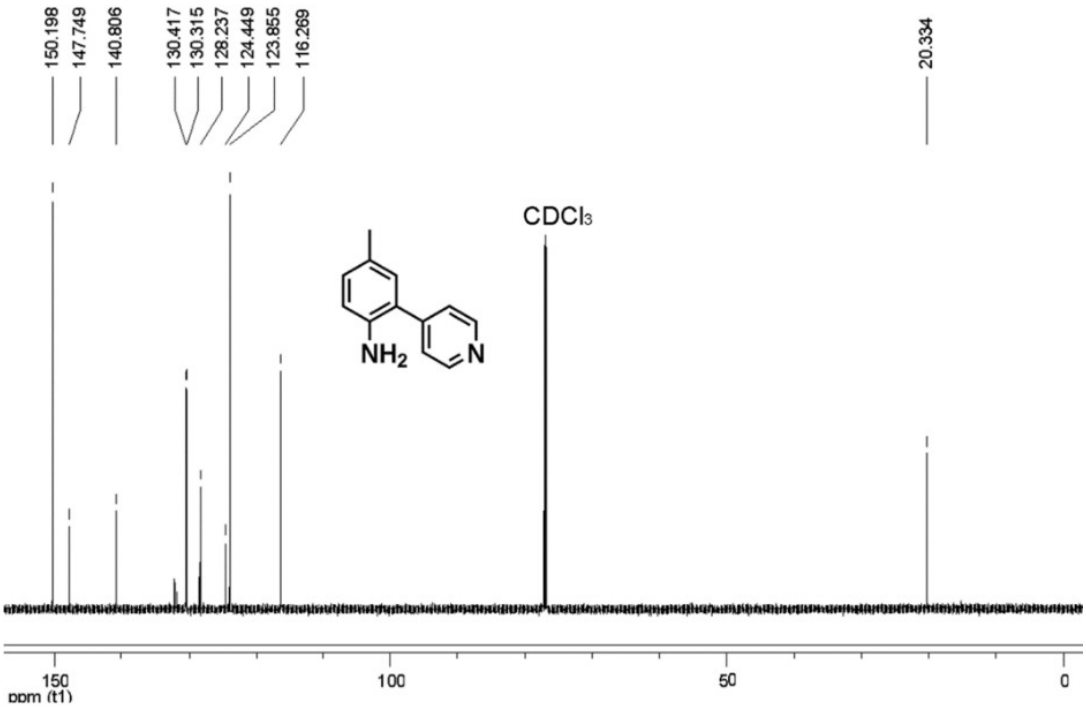

Fig. S2. ^{13}C NMR spectrum of **1** in $CDCl_3$.

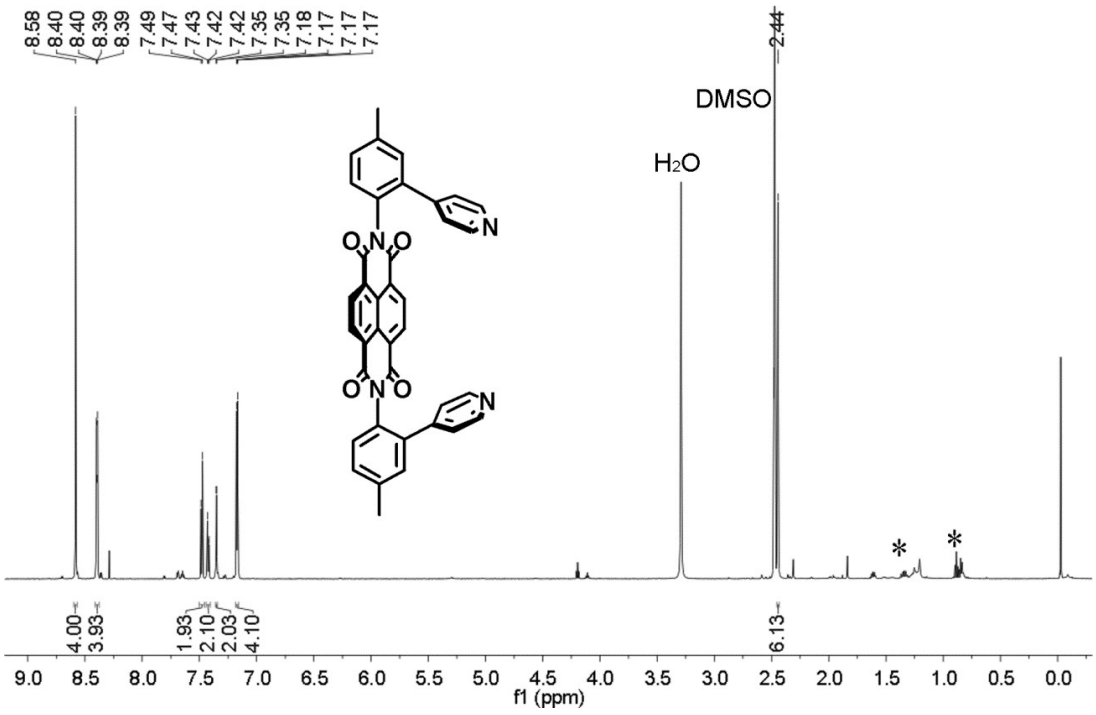

Fig. S3. ^{1}H NMR spectrum of *syn*-**A** in DMSO-d_6. The signals of small amounts of impurities are marked with *.

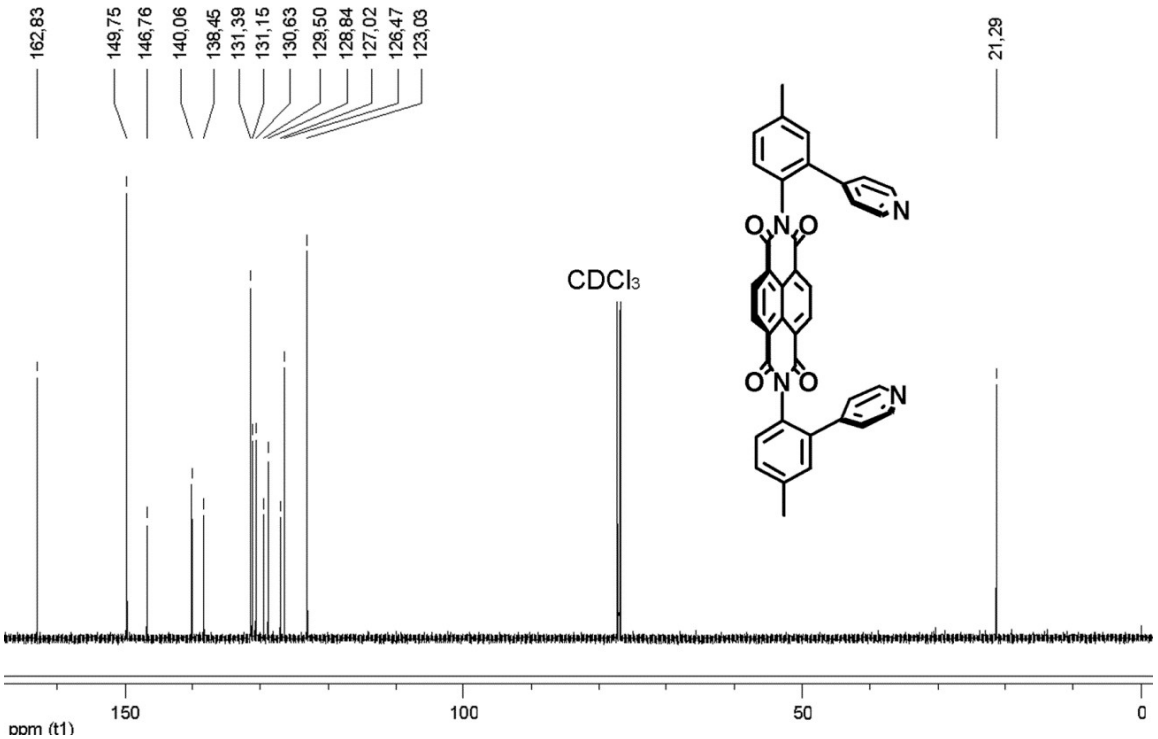

Fig. S4. ^{13}C NMR spectrum of *syn*-**A** in $CDCl_3$.

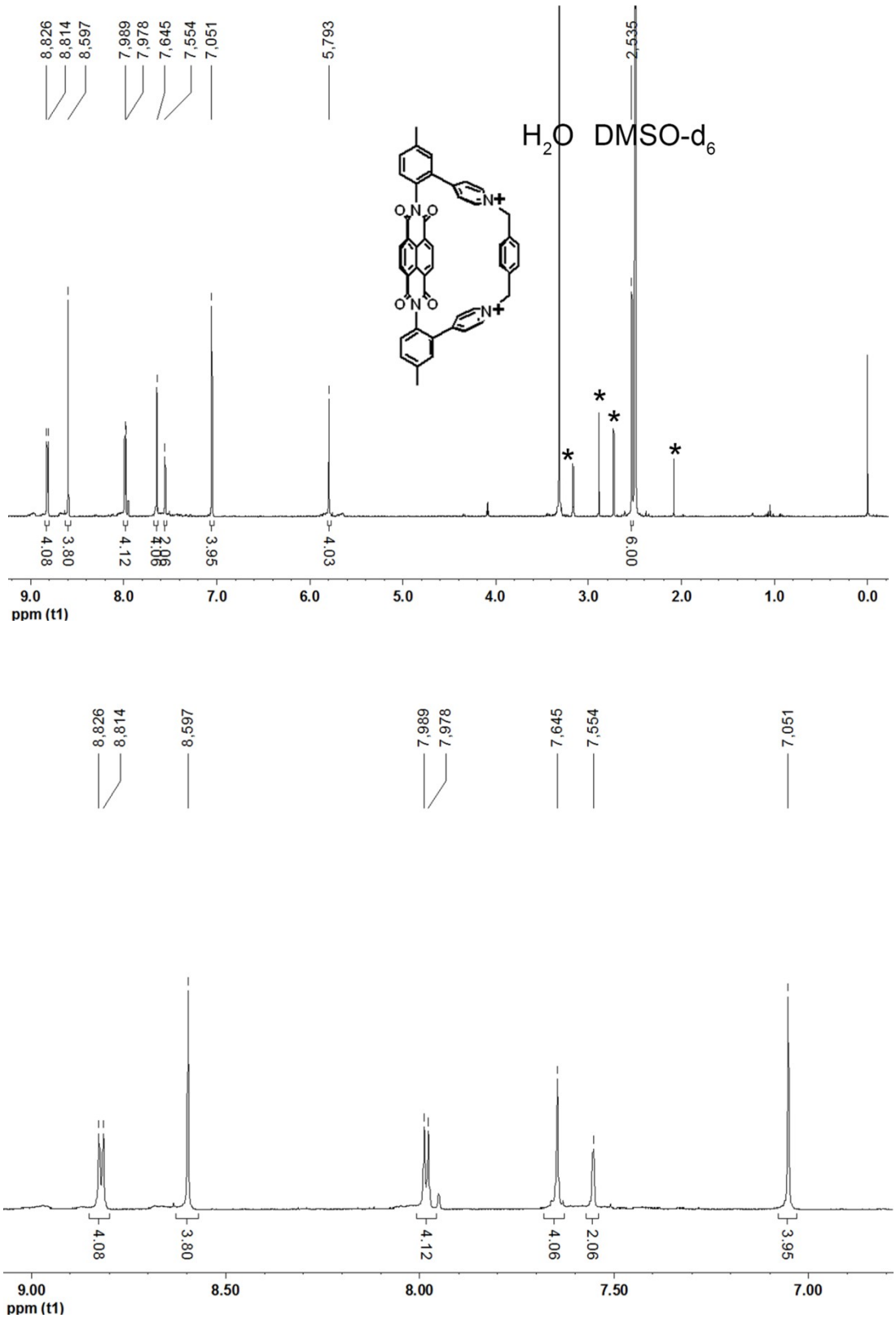

Fig. S5. ^{1}H NMR spectrum of **TBox-4**·2PF_6 in DMSO-d_6. Top: full spectrum; bottom: partial spectrum. The signals of small amounts of impurities are marked with *.

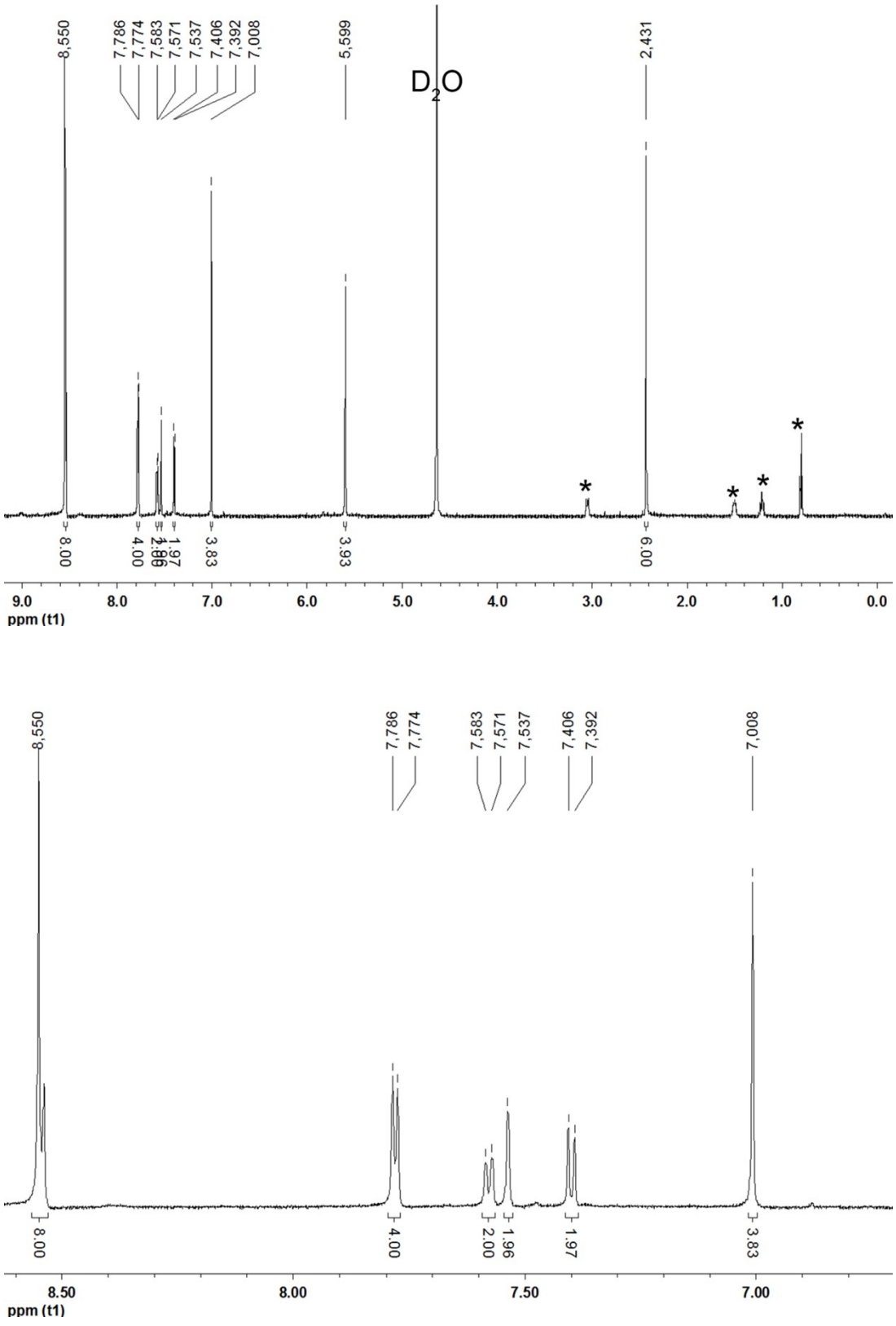

Fig. S6. ^{1}H NMR spectrum of **TBox-4**·2Br in D_2O. Top: full spectrum; bottom: partial spectrum. The signals of small amounts of impurities are marked with *.

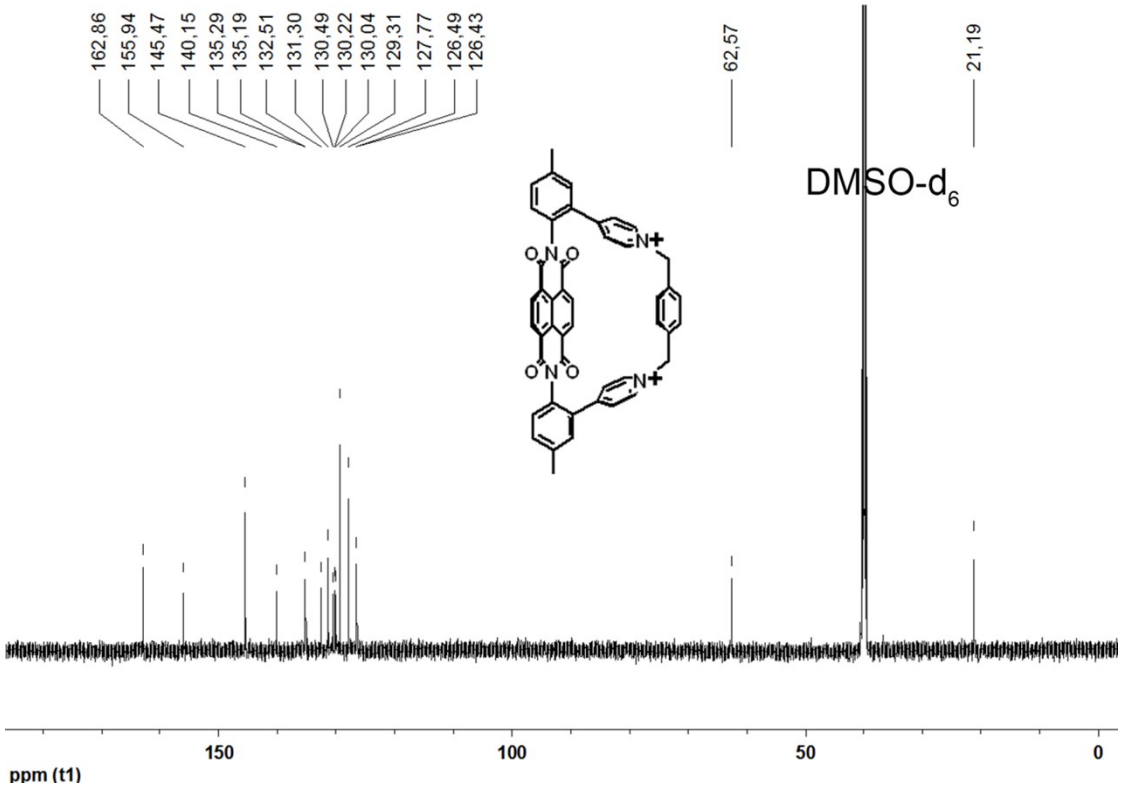

Fig. S7. ^{13}C NMR spectrum of **TBox-4**·$2PF_6$ in DMSO-d_6.

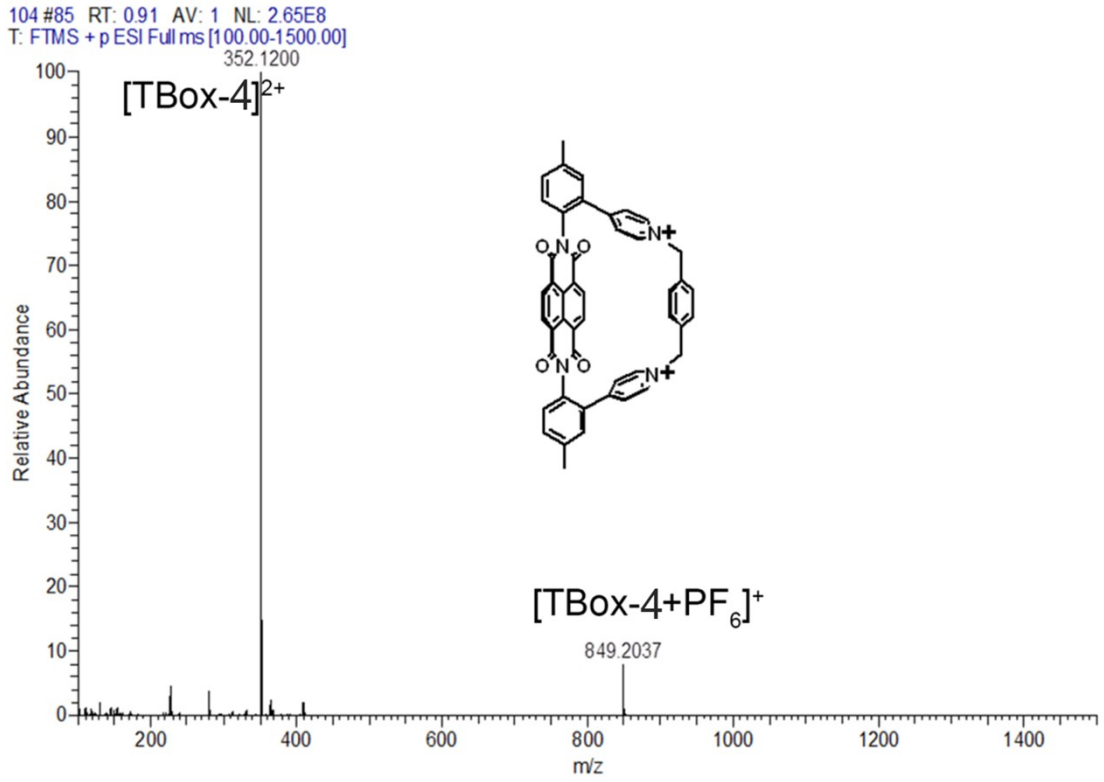

Fig. S8. HRMS of **TBox-4**·$2PF_6$.

1.3 Synthetic Routes of TBox-5^{2+}.

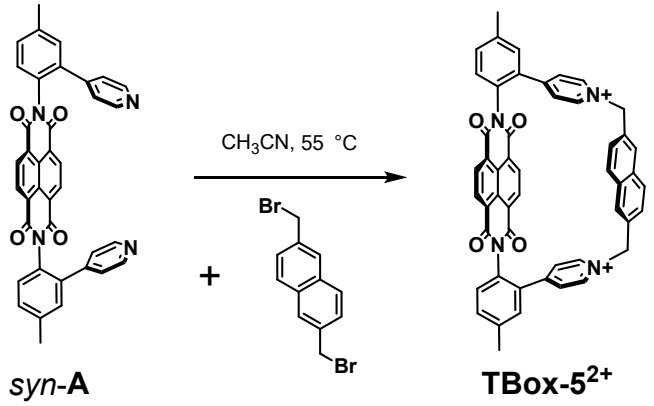

Syn-**A** (156 mg, 0.26 mmol) and 2,6-bis(bromomethyl)naphthalene (82 mg, 0.26 mmol) were stirred in dry CH_3CN at 55 °C for 5 h under nitrogen protection. The yellow precipitate was collected by vacuum filtration and dissolved in H_2O. When a saturated aqueous solution of NH_4PF_6 was added to the reaction mixture, the resulting precipitate was filtered off and then washed with deionized H_2O. The precipitate was dried to afford pure **TBox-5**·2PF_6 (203 mg, 75%) as yellowish solids without further purification. **TBox-5**·2PF_6: ^{1}H NMR (600 MHz, DMSO-d_6, 298 K): δ (ppm) = 8.887 (d, *J* = 6.6 Hz, 4H), 8.629 (s, 4H), 8.043 (d, *J* = 6.6 Hz, 4H), 7.627 (s, 2H),7.613 (s, 6H), 7.557 (s, 2H), 7.236 (d, *J* = 7.8 Hz, 2H), 6.005 (s, 4H), 2.532 (s, 6H); **TBox-5**·2Cl: ^{1}H NMR (600 MHz, D_2O, 298 K): δ (ppm) = 8.687 (d, *J* = 7.2 Hz, 4H), 8.515 (s, 4H), 7.841 (d, *J* =6.6 Hz, 4H), 7.574 (s, 2H), 7.536 (s, 2H),7.527 (s, 2H), 7.514 (s, 2H),7.277 (d, *J* = 9.0 Hz, 2H), 7.225 (d, *J* = 8.4 Hz, 2H), 5.790 (s, 4H), 2.421 (s, 6H); ^{13}C NMR (150 MHz, DMSO-d_6, 298 K): δ (ppm) = 162.89, 155.87, 145.82, 140.18, 135.42, 134.13,132.67, 132.59, 131.33, 130.73, 130.63, 130.32, 129.31, 127.91,127.59,126.77 (C of phenyl and pyridyl), 63.21 (C of methylene), 21.14 (C of methyl). HRMS (ESI) *m/z* calcd for [**TBox-5**]$^{2+}$: 377.1285, found: 377.1287. Single crystals were grown by slow diffusion of diethyl ether into an MeCN solution of **TBox-5**·2PF_6 over 3 days.

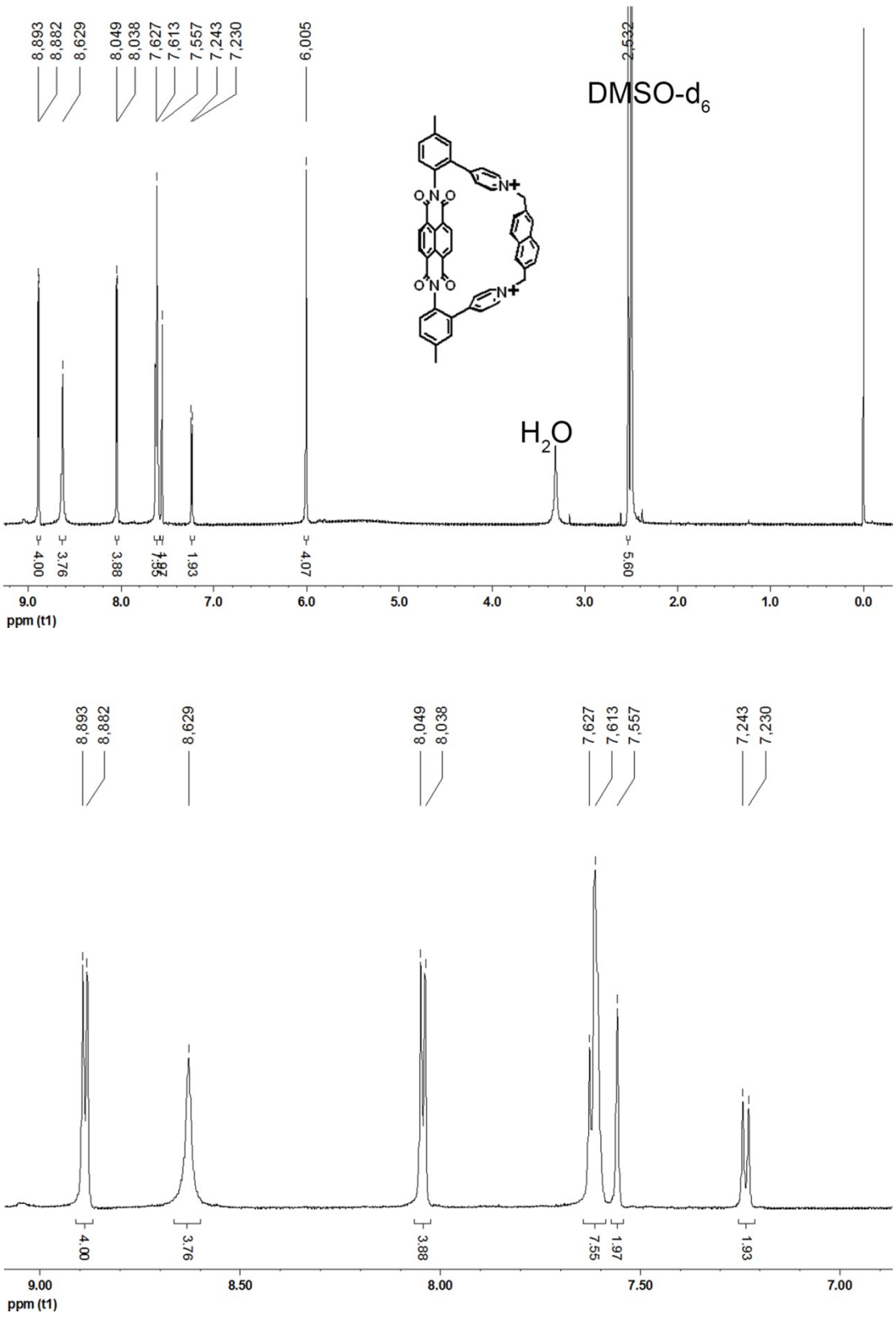

Fig. S9. ^{1}H NMR spectrum of **TBox-5**·2PF_6 in DMSO-d_6. Top: full spectrum; bottom: partial spectrum.

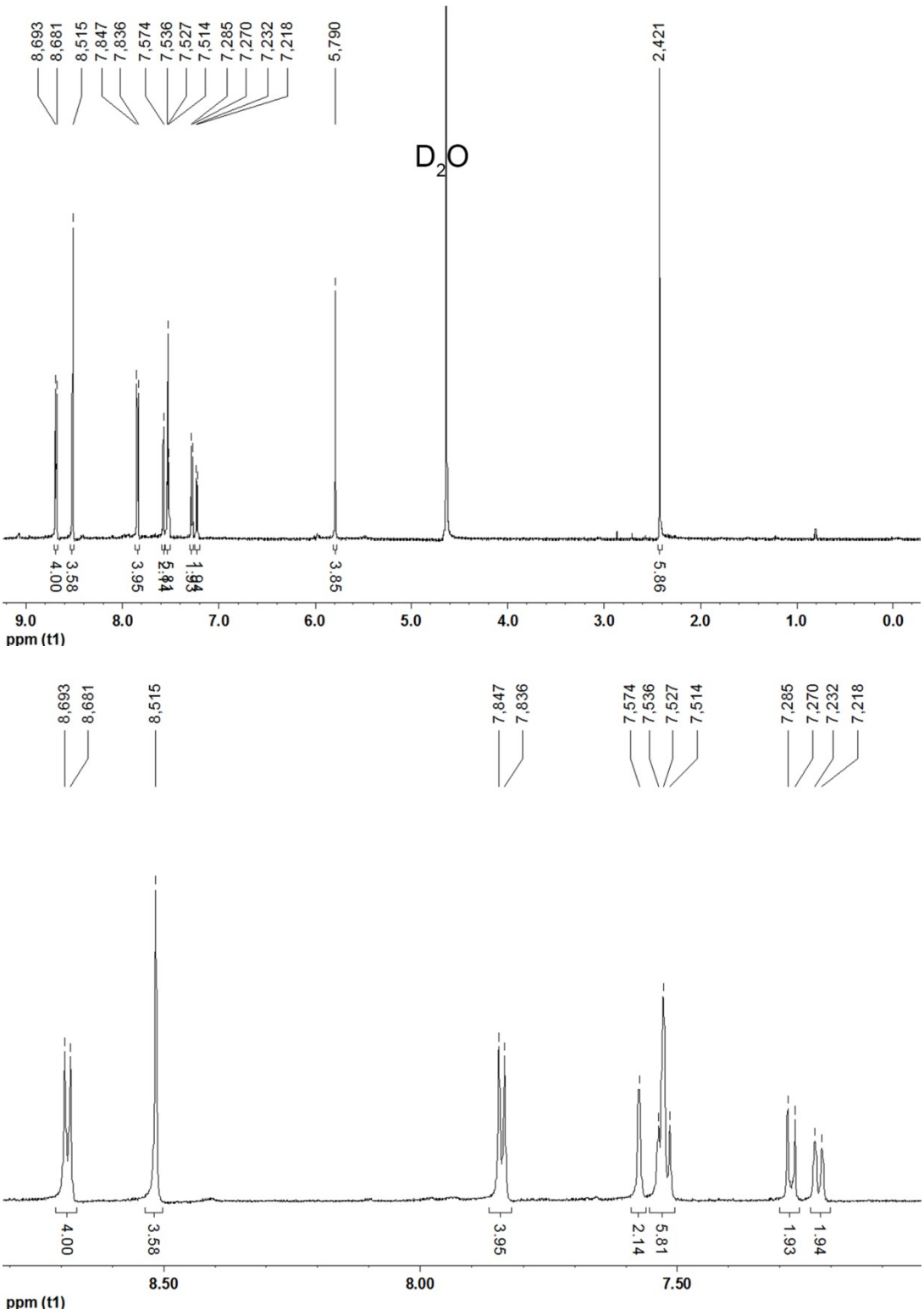

Fig. S10. ^{1}H NMR spectrum of **TBox-5**·2Cl in D_2O. Top: full spectrum; bottom: partial spectrum.

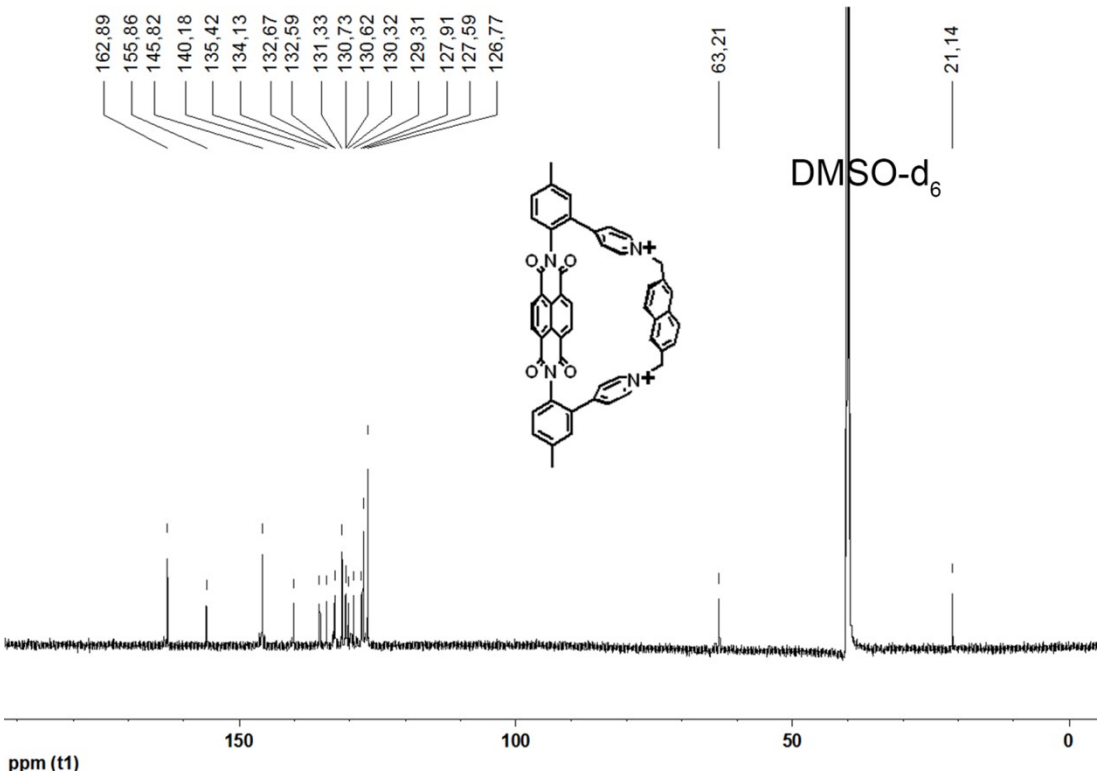

Fig. S11. ^{13}C NMR spectrum of **TBox-5**·2PF$_6$ in DMSO-d$_6$.

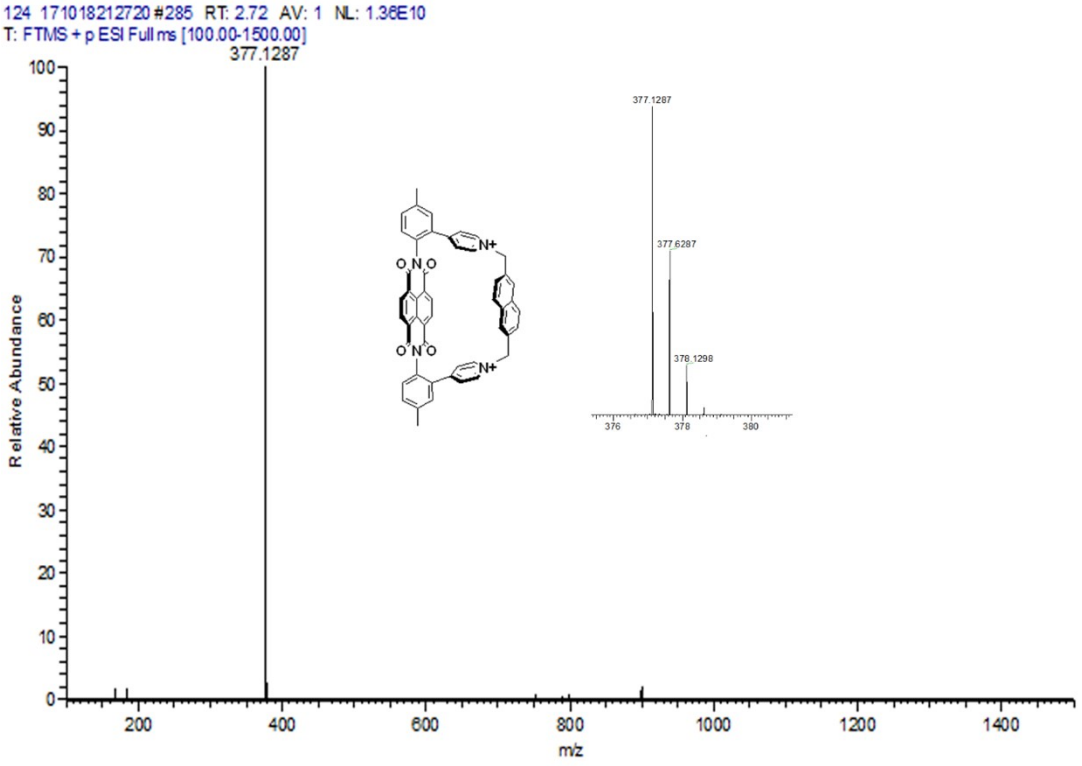

Fig. S12. HRMS of **TBox-5**·2PF$_6$.

1.4 Synthetic Routes of TBox-6^{2+}.

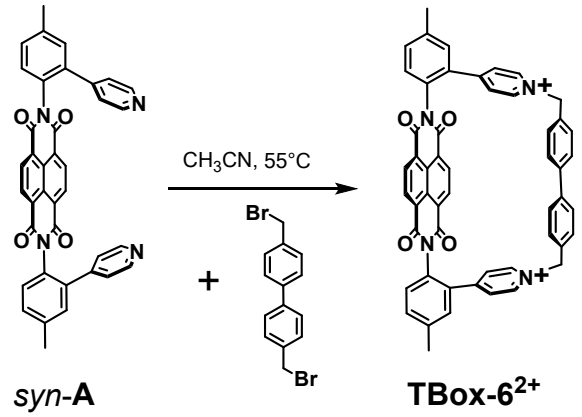

Syn-**A** (156 mg, 0.26 mmol) and 4,4'-bis(bromomethyl) diphenyl (88 mg, 0.26 mmol) were stirred in dry CH_3CN at 55 °C for 10 h under nitrogen protection. The yellow precipitate was collected by vacuum filtration and dissolved in H_2O. When a saturated aqueous solution of NH_4PF_6 was added to the reaction mixture, the resulting precipitate was filtered off and then washed with deionized H_2O. The precipitate was dried to afford pure **TBox-6**·2PF_6 (180 mg, 65%) as yellowish solids without further purification. **TBox-6**·2PF_6: ^{1}H NMR (600 MHz, DMSO-d_6, 298 K): δ (ppm) = 8.909 (d, *J* = 10.8 Hz, 4H), 8.571 (s, 4H), 8.042 (d, *J* = 10.8 Hz, 4H), 7.688 (d, *J* = 12.6 Hz, 4H), 7.585 (s, 4H), 7.524 (s, 4H), 7.502 (s, 2H), 5.844 (s, 4H); **TBox-6**·2Cl: ^{1}H NMR (600 MHz, D_2O, 298 K): δ (ppm) = 8.365 (d, *J* = 9.6 Hz, 4H), 7.875 (s, 4H), 7.678 (d, *J* =9.6 Hz, 4H), 7.644 (d, *J* =12.6 Hz, 2H), 7.602 (s, 2H),7.293 (s, 2H), 7.274 (s, 4H),7.255 (s, 4H), 5.565 (s, 4H), 2.505 (s, 6H); ^{13}C NMR (150 MHz, DMSO-d_6, 298 K): δ (ppm) = 163.53, 155.37, 145.17, 140.27, 139.47, 135.54, 134.43, 132.81, 131.86, 131.20, 131.16, 130.94, 130.60, 127.55, 127.30, 127.20 (C of phenyl and pyridyl), 63.25 (C of methylene), 21.08 (C of methyl). HRMS (ESI) *m/z* calcd for [**TBox-6**]$^{2+}$: 390.1363, found: 390.1359, *m/z* calcd for [**TBox-6**+PF_6]$^+$: 925.2373, found: 925.2350. Single crystals were grown by slow diffusion of ethyl acetate into an MeCN solution of **TBox-6**·2PF_6 over 3 days.

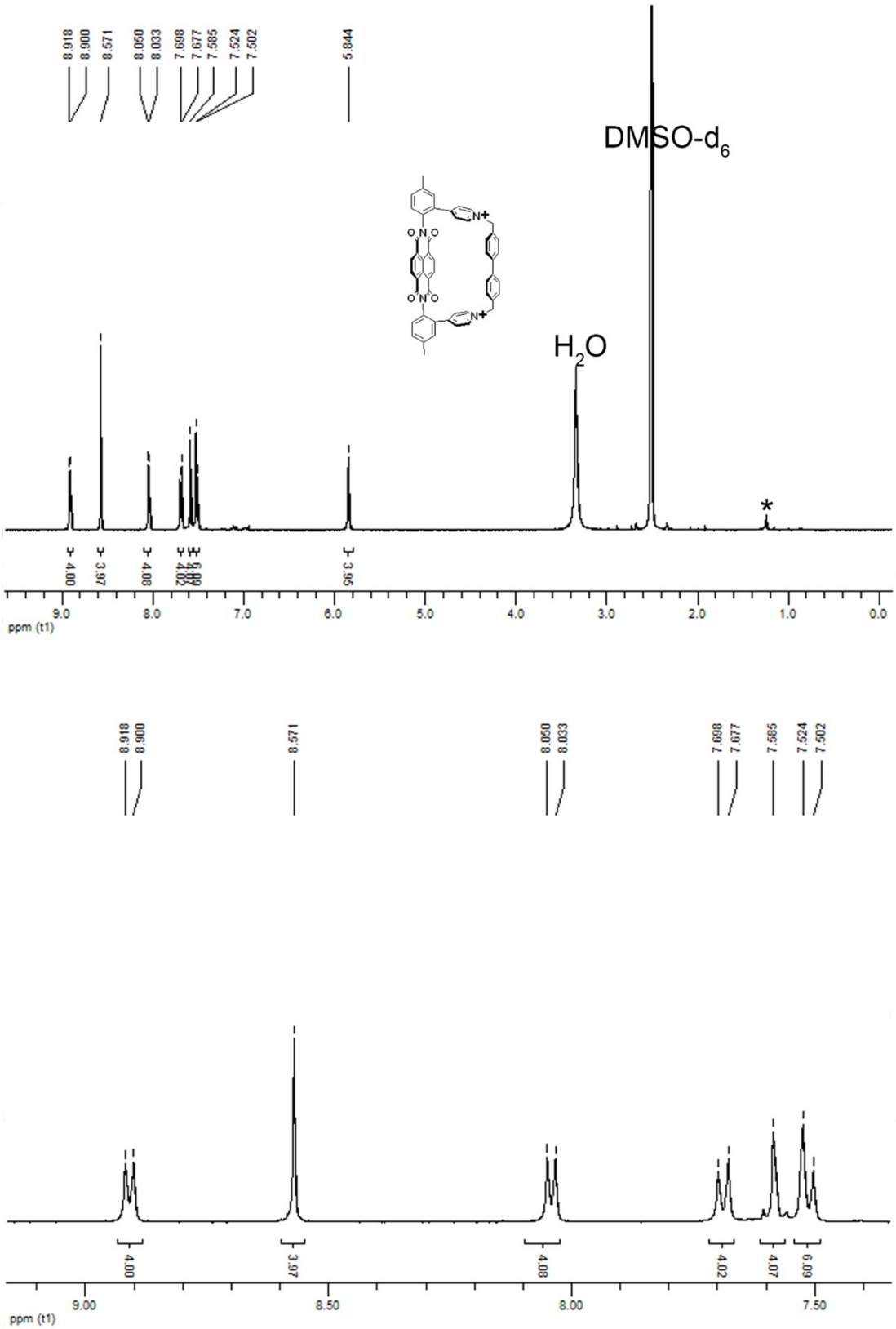

Fig. S13. ^{1}H NMR spectrum of **TBox-6**·2PF_6 in DMSO-d_6. Top: full spectrum; bottom: partial spectrum. The signals of small amounts of impurities are marked with *.

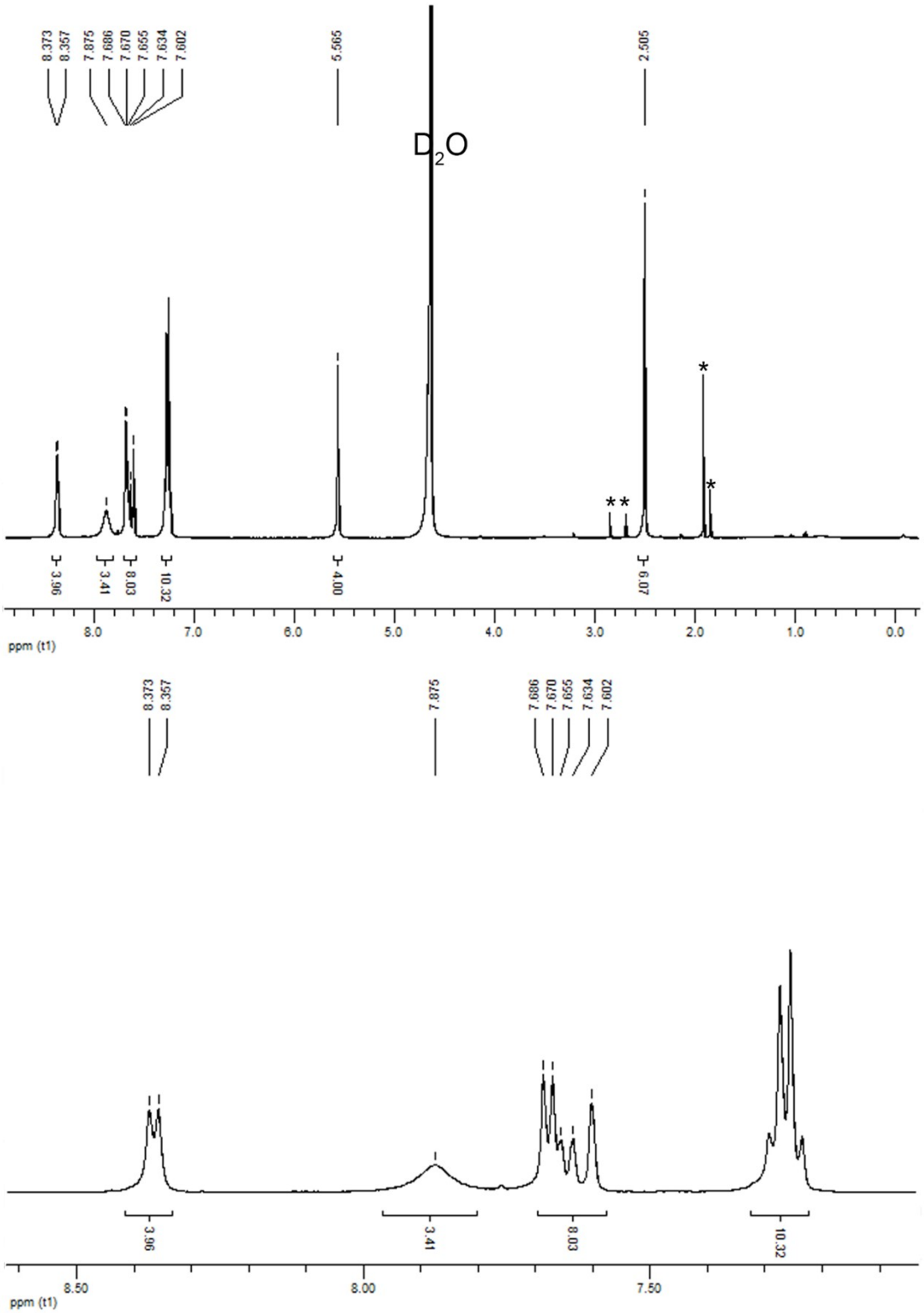

Fig. S14. ^{1}H NMR spectrum of **TBox-6**·2Cl in D_2O. Top: full spectrum; bottom: partial spectrum. The signals of small amounts of impurities are marked with *.

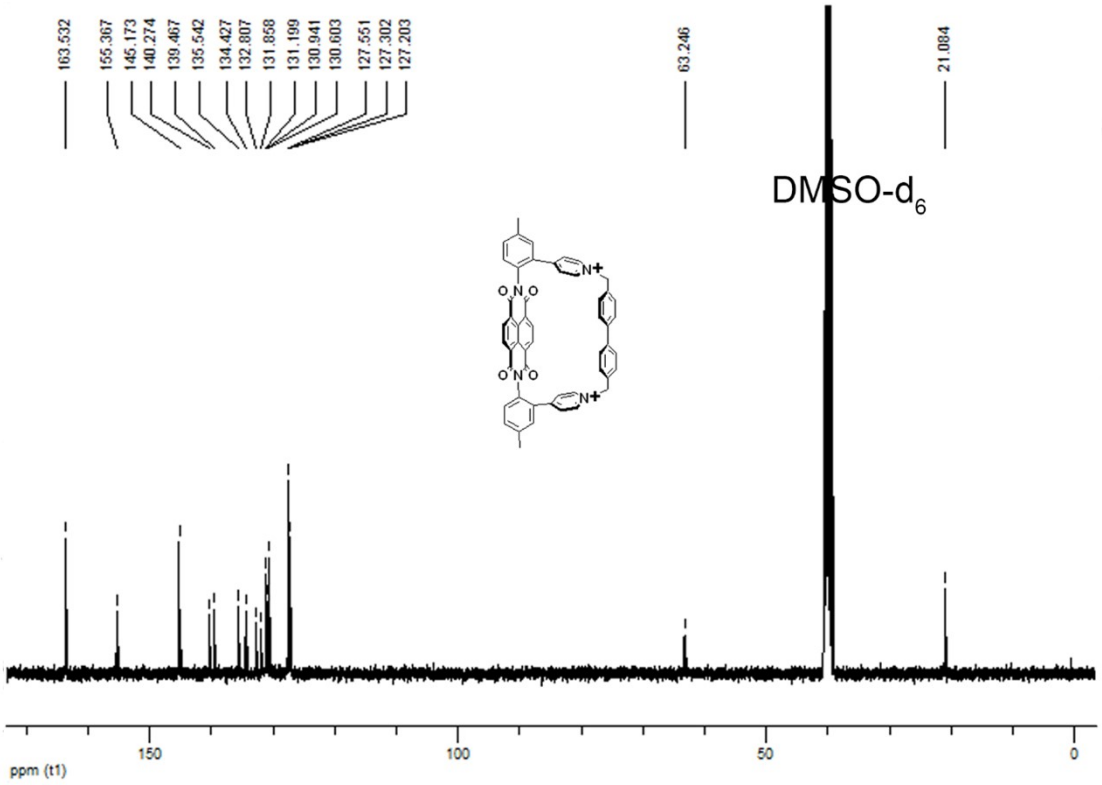

Fig. S15. ^{13}C NMR spectrum of **TBox-6**·2PF_6 in DMSO-d_6.

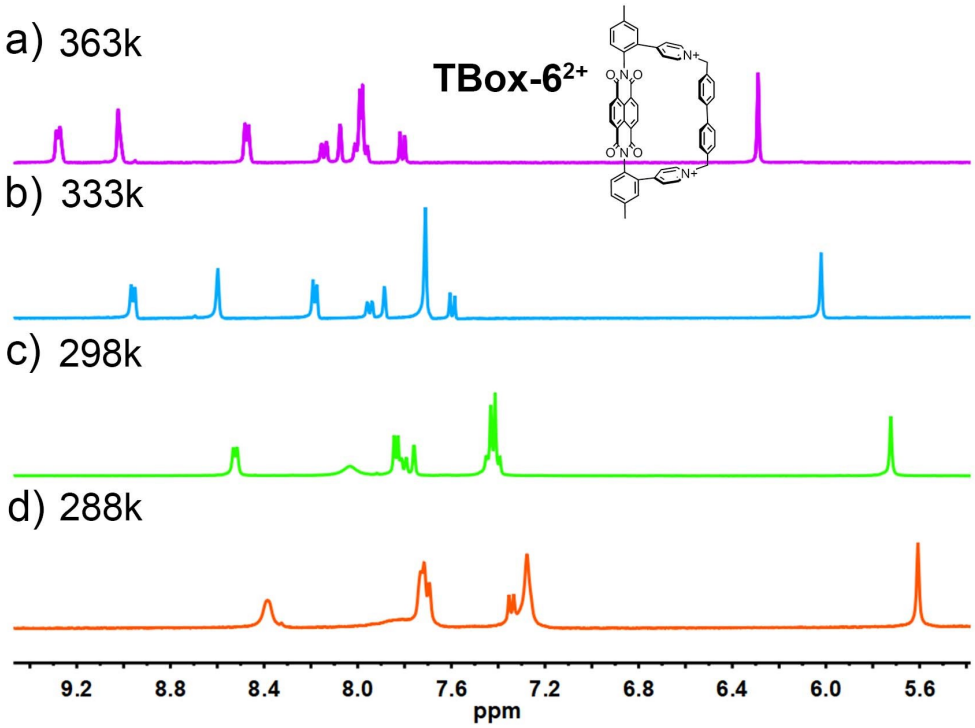

Fig. S16. Temperature-dependent ^{1}H NMR spectra for **TBox-6**·2Cl in D_2O. The measurements were performed in the range of 288–363 K

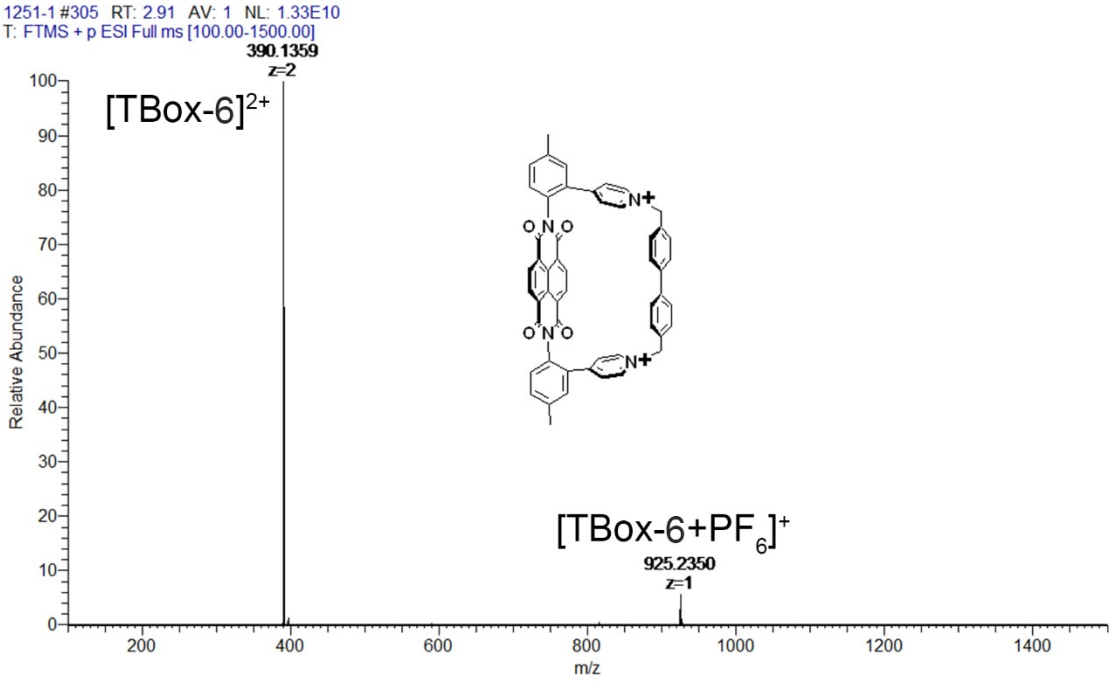

Fig. S17. HRMS of **TBox-6**·2PF_6.

2. Determination of Rotational Barrier of Atropisomer Precursor

Syn-**A** (12 mg) was dissolved in DMSO-d_6 (0.6 mL), and was kept at 80 °C. The ratio of the two isomers was determined by standard deconvolution of the pyridyl protons at 8.415 ppm for *syn*-**A** and 8.380 ppm for *anti*-**A**. The ln[(R-R_e)/(R+1) of was plotted versus time (s), where R_e is the ratio of *syn*/*anti* isomers at equilibrium and R the ratio of *syn*/*anti* at time t seconds. The slope of this plot corresponds to the observed rate k_{obs}, where k_{obs} is equal to 4k, and k is the rate of rotation of a single rotor for a reversible reaction. The 4 accounts for the reversibility of the system (the forward and the reverse rate constants) and the two rotors. Then using the Eyring equation $k = \frac{k_B T}{h} e^{-\frac{\Delta G^{\ddagger}}{RT}}$, the rotational barrier can be determined. The energy of rotation was calculated to be 27.42 kcal/mol at 80 °C. The half-life $t_{1/2}$ equals (ln2)/(4k). Thus, $t_{1/2}$ at 80°C is 38 min, while $t_{1/2}$ at 60 °C is 416 min.

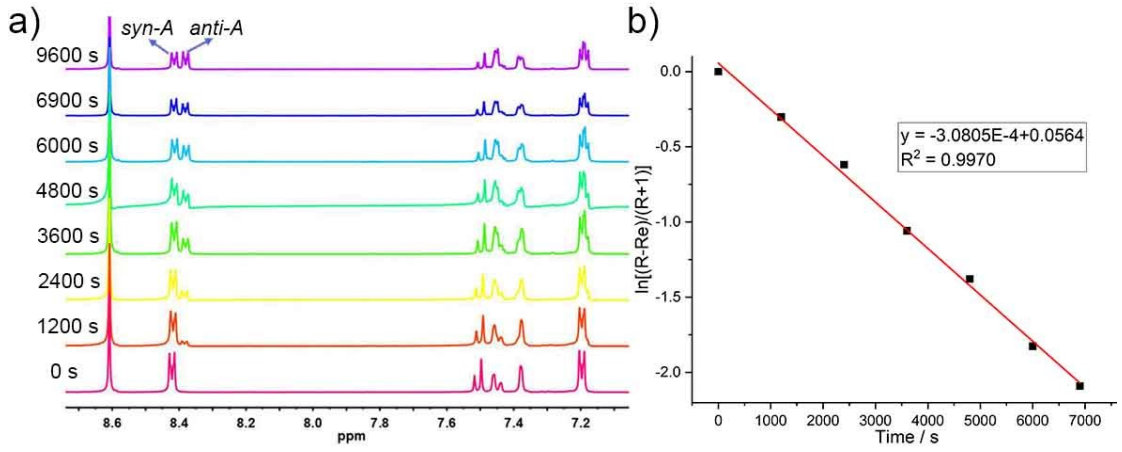

Fig. S18. a) ^{1}H NMR signals of the pyridyl protons for *syn*-**A** and *anti*-**A** at 80 °C. b) Rotational barrier determination via isomeric equilibration.

3. Single Crystal X-Ray Crystallography

Data collections for *syn*-**A**, **TBox-4**$^{2+}$, **TBox-5**$^{2+}$ were performed on a Rigaku XtaLAB PRO MM007 diffractometer equipped with a graphite monochromated Cu-Kα radiation (λ = 1.54184 Å). An absorption correction was applied using the SADABS program.[S1] The structures were solved by direct methods and refined on F^2 by full-matrix least-squares using the *SHELXTL*-97 program package.[S2] The ordered atoms in each structure were refined with anisotropic displacement parameters, while the hydrogen atoms were placed in idealized positions and allowed to ride on the relevant carbon atoms. A summary of the crystallographic data was presented in Table S1. CCDC-2107206 (*syn*-**A**), CCDC-1875218 (**TBox-4**$^{2+}$) and CCDC-1875217 (**TBox-5**$^{2+}$) contain the supplementary crystallographic data for this paper. These data can be obtained free of charge from The Cambridge Crystallographic Data Centre *via* www.ccdc.cam.ac.uk/data_request/cif.

The water molecule near Mg^{2+} in the crystal of *syn*-**A** was disordered and refined in two split positions with reduced site occupation factors, which lead to the alert (PLAT420_ALERT_2_B) in the checkCIF report. The large solvent accessible void (PLAT602_ALERT_2_A) of one-dimensional channel in *syn*-**A** is probably due to the stable and flexible structure, held together by multiple weak interactions including π-π stacking, hydrogen bonding and coordination interaction. Because of the very large thermal motion and disorder of the solvents in the lattice, the diffuse residual electron density is difficult to be accurately modeled and thus a treatment by SQUEEZE (from PLATON) was used for solvate molecule in **TBox-4**$^{2+}$ and **TBox-5**$^{2+}$, which leads to large solvent accessible voids in structures.

Table S1. Crystal data and structure refinements for all the complexes.

	syn-**A**	**TBox-4**$^{2+}$	**TBox-5**$^{2+}$
formula	$C_{38}H_{32}N_6O_{14}Mg_1$	$C_{92}H_{64}N_8O_8P_4F_{24}$	$C_{50}H_{34}N_4O_4P_2F_{12}$
Mr.	821.00	1989.39	1044.75
crystal system	triclinic	monoclinic	monoclinic
space group	*P*-1	$P2_1$	$P2_1/n$
a [Å]	9.0813(2)	13.0593(2)	12.3869(3)
b [Å]	15.6295(3)	29.9001(5)	25.3788(6)
c [Å]	16.8870(3)	13.7754(2)	16.9113(4)
α [°]	64.472(2)	90	90
β [°]	85.9190(10)	106.534(2)	108.419(3)
γ [°]	80.7210(10)	90	90
V [A^3]	2134.58(8)	5156.53(15)	5044.0(2)
Z	2	2	4
D_{calcd} [Mg/m^3]	1.277	1.281	1.376
measured refl.	23577	32430	29785
unique refl.	8345	15471	9940
R_{int}	0.0401	0.0442	0.0517
GooF	1.045	1.069	1.084
R_1, wR_2 [$I > 2\sigma(I)$]	0.0456, 0.1197	0.0621, 0.1696	0.0659, 0.1837
R_1, wR_2 [all data]	0.0530, 0.1236	0.0695, 0.1750	0.0738, 0.1897

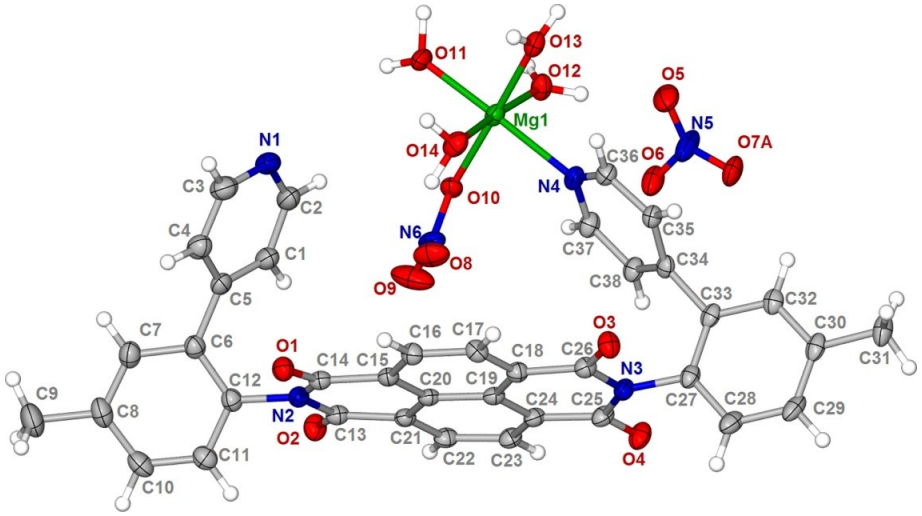

Fig. S19. Single crystal structure of *syn*-**A**. The asymmetric unit was labeled, and the C, N, O and Br atoms are drawn as 50% thermal ellipsoids. Disordered water and NO_3^- moiety were omitted for clarity.

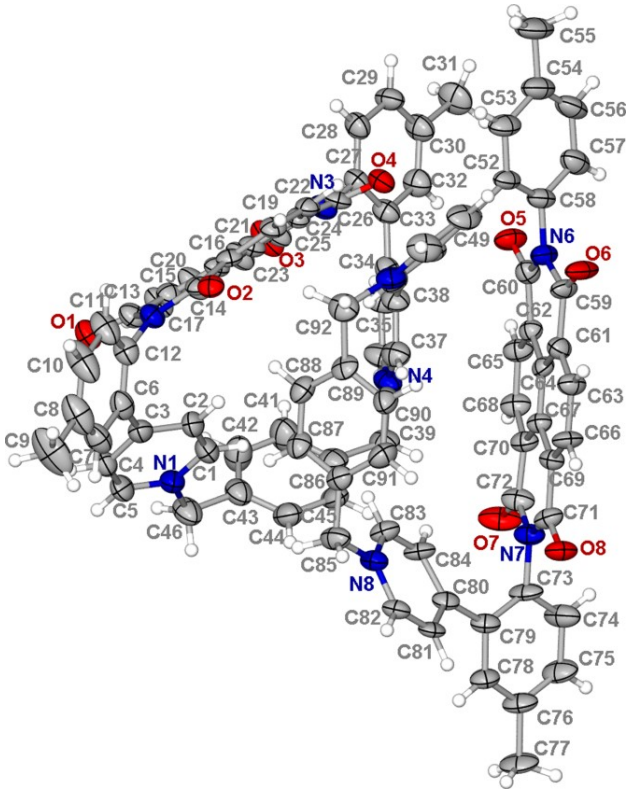

Fig. S20. Single crystal structure of **TBox-4**$^{2+}$. The asymmetric unit was labeled, and the C, N, and O atoms are drawn as 50% thermal ellipsoids. Disordered PF_6^- ions were omitted for clarity.

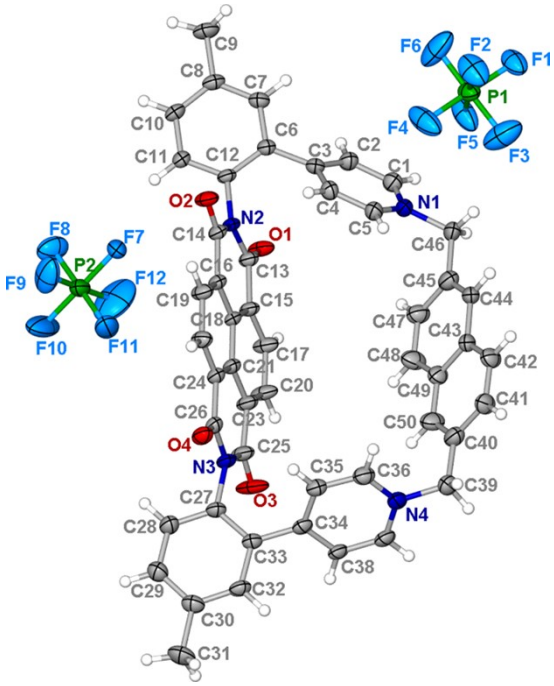

Fig. S21. Single crystal structure of **TBox-5**$^{2+}$. The asymmetric unit was labeled, and the C, N, P, F and O atoms are drawn as 50% thermal ellipsoids. Disordered naphthyl and PF_6^- moieties were omitted for clarity.

4. Theoretical calculations for TBox-6^{2+} .

For the reason that we failed to get enough quality of crystalline sample **Tbox-6^{2+}** to collect the corresponding diffraction data, the density functional theory (DFT) calculation was carried out for **TBox-6^{2+}** using the Gaussian 09 program.[S3] PCM solvation model[S4] was used in all calculations. The geometry optimizations were carried out using B3LYP/6-31G(d)[S5] level of theory with Grimme's D3 dispersion correction[S6] based upon the crystal data of **TBox-5^{2+}**.

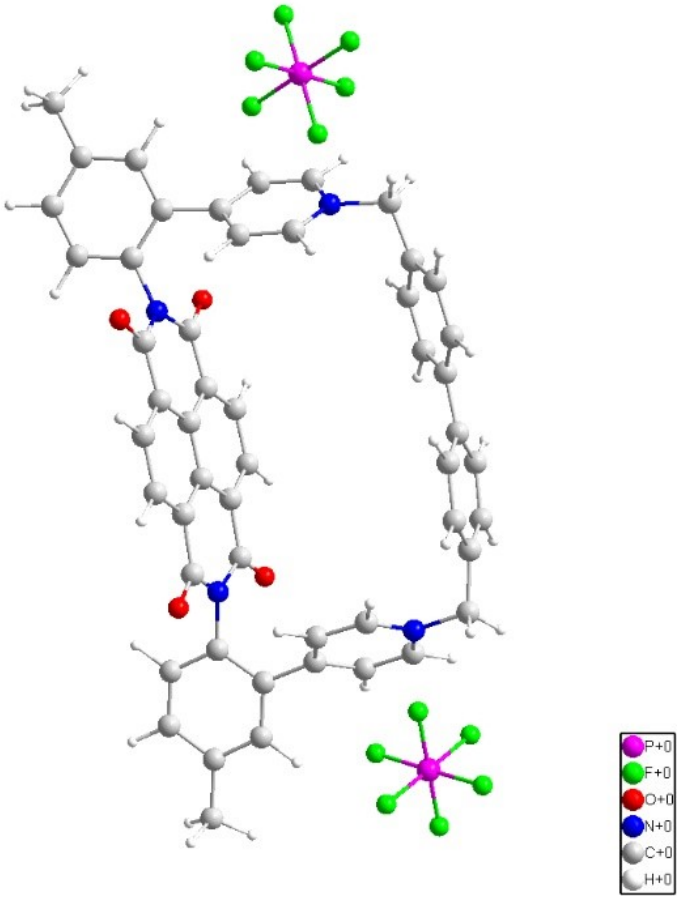

Fig. S22. Optimized structure of **TBox-6^{2+}** at the B3LYP-D3/6-31G(d)/PCM level of theory.

5. Characterization of Host-Guest Properties

The association constant (K_a) for the formation of the 1:1 complex between guest molecules and **TBox-4**$^{2+}$–**TBox-6**$^{2+}$ were determined by UV-Vis or ^{1}H NMR titration experiments. For the ^{1}H NMR titration experiments, a solution of **TBox-4**$^{2+}$ (1.41×10^{-3} M) was prepared in D_2O. This solution (0.4 mL) was placed in a NMR tube. The sample was then titrated with a solution of guest. NMR titrations were performed by adding guest to the solution of host with a fixed concentration. The nonlinear curve-fitting method was then used to obtain the binding constants through the following equation:

$$\Delta\delta = \Delta\delta^*\{0.5^*G_0+0.5^*(H_0+1/K_a)–\text{sqrt}[0.25^*(H_0+G_0+1/K_a)\text{^}2–H_0^*G_0]\}$$

For the UV-Vis titration experiments, when the solution of guest was added incrementally to the solution of **TBox-5**$^{2+}$ or **TBox-6**$^{2+}$, the UV-Vis spectra were recorded one after the other. The stacked spectra show that, upon the addition of guest, new absorption bands emerge and are enhanced. The nonlinear curve-fitting method was then used to obtain the association constant through the following equation:

$$\Delta A = \Delta\varepsilon^*\{0.5^*G_0+0.5^*(H_0+1/K_a)–\text{sqrt}[0.25^*(H_0+G_0+1/K_a)\text{^}2–H_0^*G_0]\}$$

where ΔA is the change in the absorbance on gradual addition of guest, whereas $\Delta\varepsilon$ refers to the difference of molar absorptivity between host-guest complexes and free hosts; the total concentration of **TBox**$^{2+}$ and guest is denoted by H_0 and G_0. From the UV-vis titration experiments, plots of absorption intensity against the guest concentrations were obtained and nonlinear least squares data treatments (red line) gave the corresponding association constants of host-guest complexes.[S7]

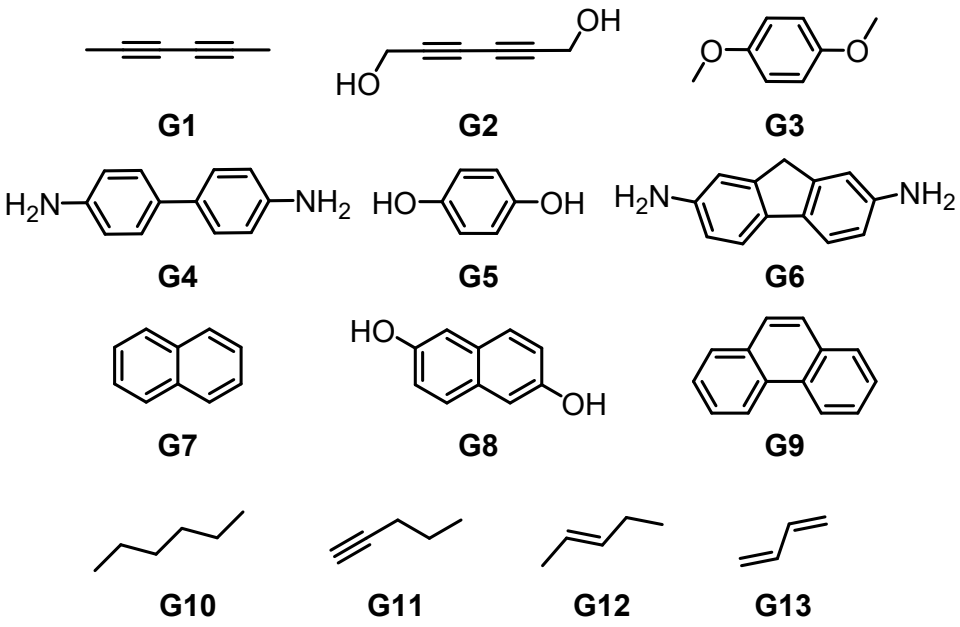

Fig. S23. Chemical structures of the investigated guests **G1-G13**.

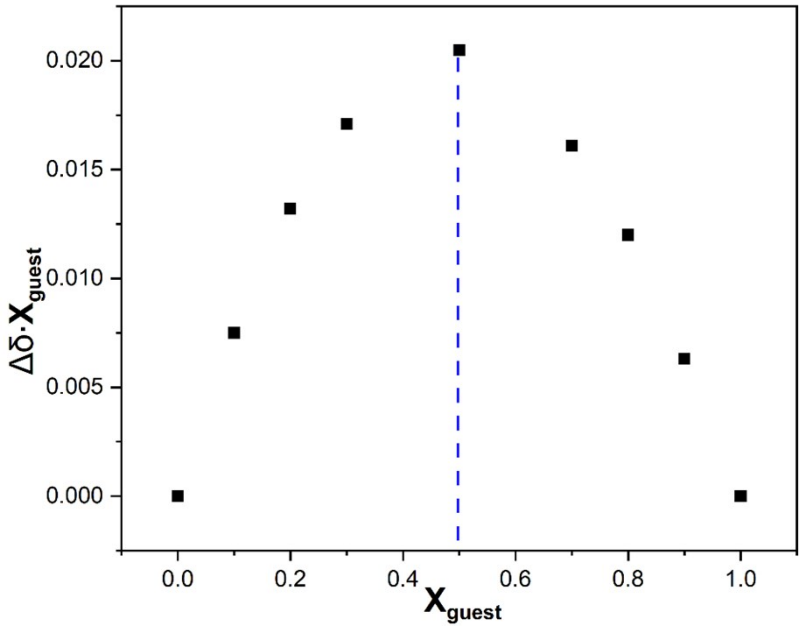

Fig. S24. Job-plot analysis of binding complex between **TBox-4**$^{2+}$ and **G2** from ^{1}H NMR. Job-plot corresponding to the binding between **TBox-4**$^{2+}$ and **G2** at different molarity ratio with a fixed total concentration ([**TBox-4**$^{2+}$] + [**G2**] =2.7 mM). The value distribution indicates a 1:1 (host:guest) binding stoichiometry in D_2O.

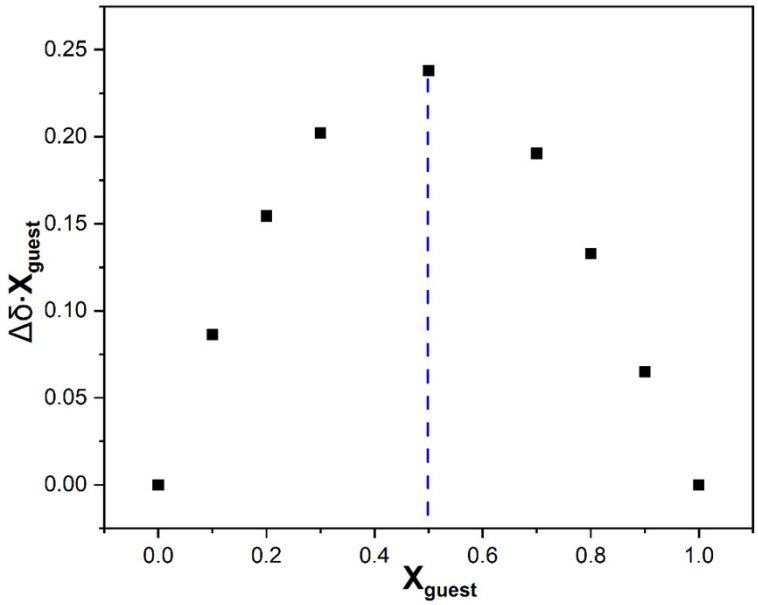

Fig. S25. Job-plot analysis of binding complex between **TBox-5**$^{2+}$ and **G5** from ^{1}H NMR. Job-plot corresponding to the binding between **TBox-5**$^{2+}$ and **G5** at different molarity ratio with a fixed total concentration ([**TBox-5**$^{2+}$] + [**G5**] =2.1 mM). The value distribution indicates a 1:1 (host:guest) binding stoichiometry in D_2O.

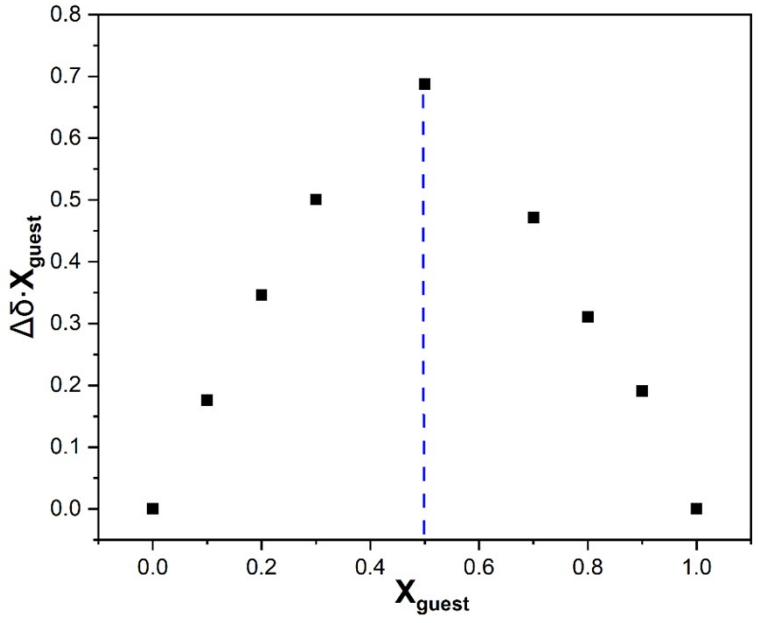

Fig. S26. Job-plot analysis of binding complex between **TBox-6**$^{2+}$ and **G8** from ^{1}H NMR. Job-plot corresponding to the binding between **TBox-6**$^{2+}$ and **G8** at different molarity ratio with a fixed total concentration ([**TBox-6**$^{2+}$] + [**G8**] =2.2 mM). The value distribution indicates a 1:1 (host:guest) binding stoichiometry in D_2O.

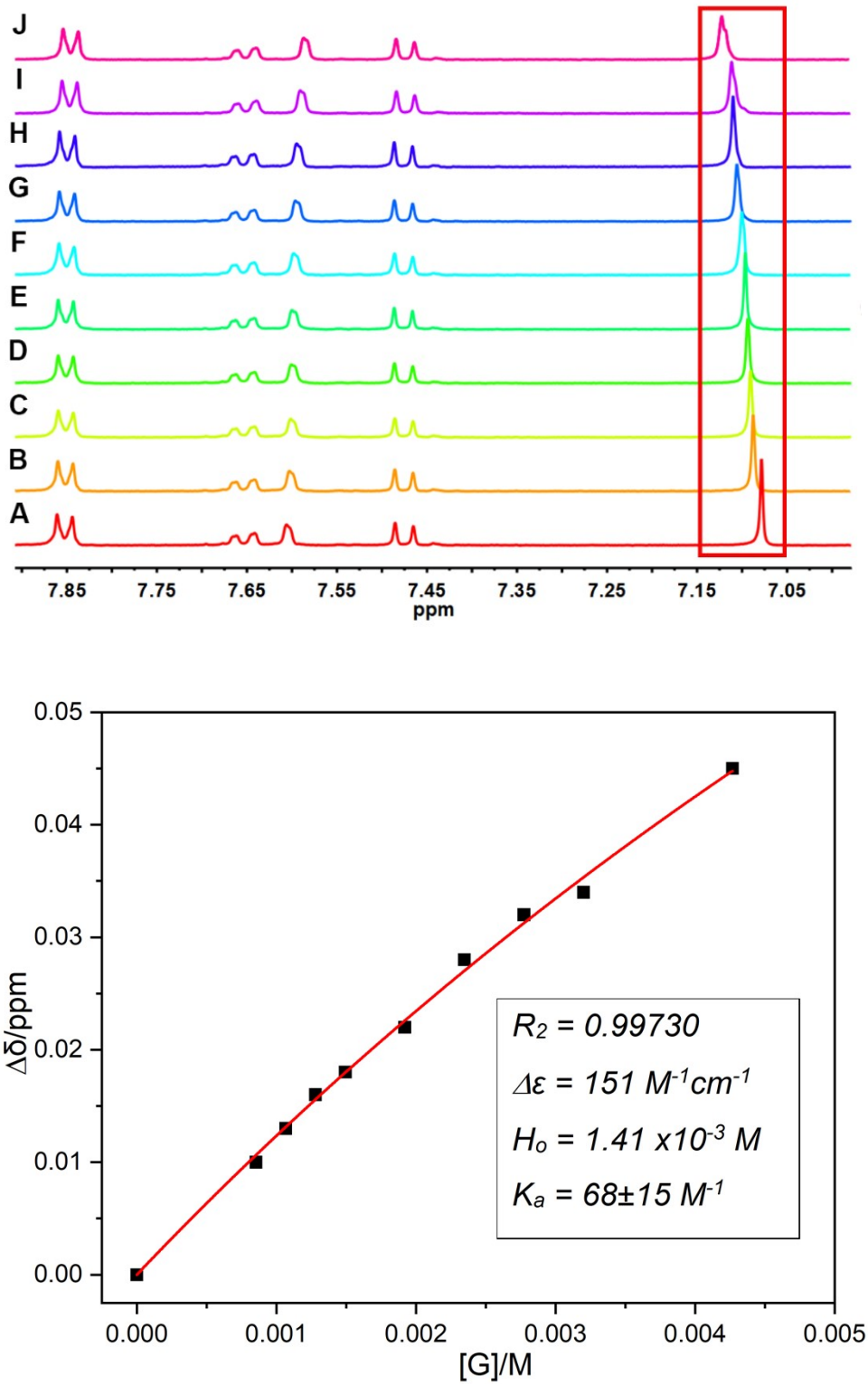

Fig. S27. Top: stacked ^{1}H NMR spectra (600 MHz, D_2O, 298 K) obtained by titrating **G1** into an aqueous solution of **TBox-4**·2Cl (1.41×10^{-3} M). Bottom: the nonlinear curve-fitting for the complexation of **TBox-4**$^{2+}$ with **G1** to give an association constant of 68 ± 15 M^{-1}.

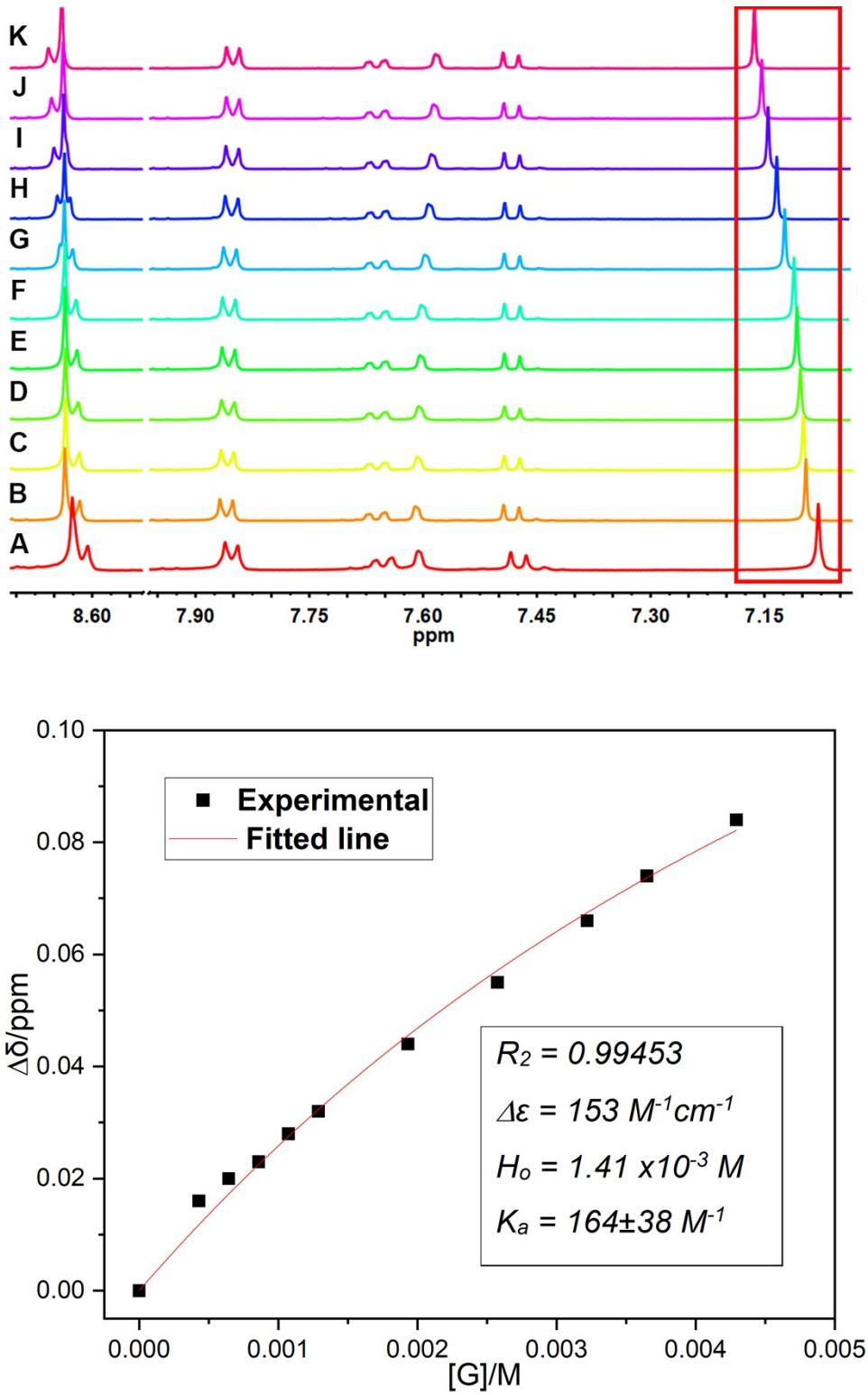

Fig. S28. Top: stacked ^{1}H NMR spectra (600 MHz, D_2O, 298 K) obtained by titrating **G2** into an aqueous solution of **TBox-4**·2Cl (1.41×10^{-3} M). Bottom: the nonlinear curve-fitting for the complexation of **TBox-4**$^{2+}$ with **G2** to give an association constant of 164 ± 38 M^{-1}.

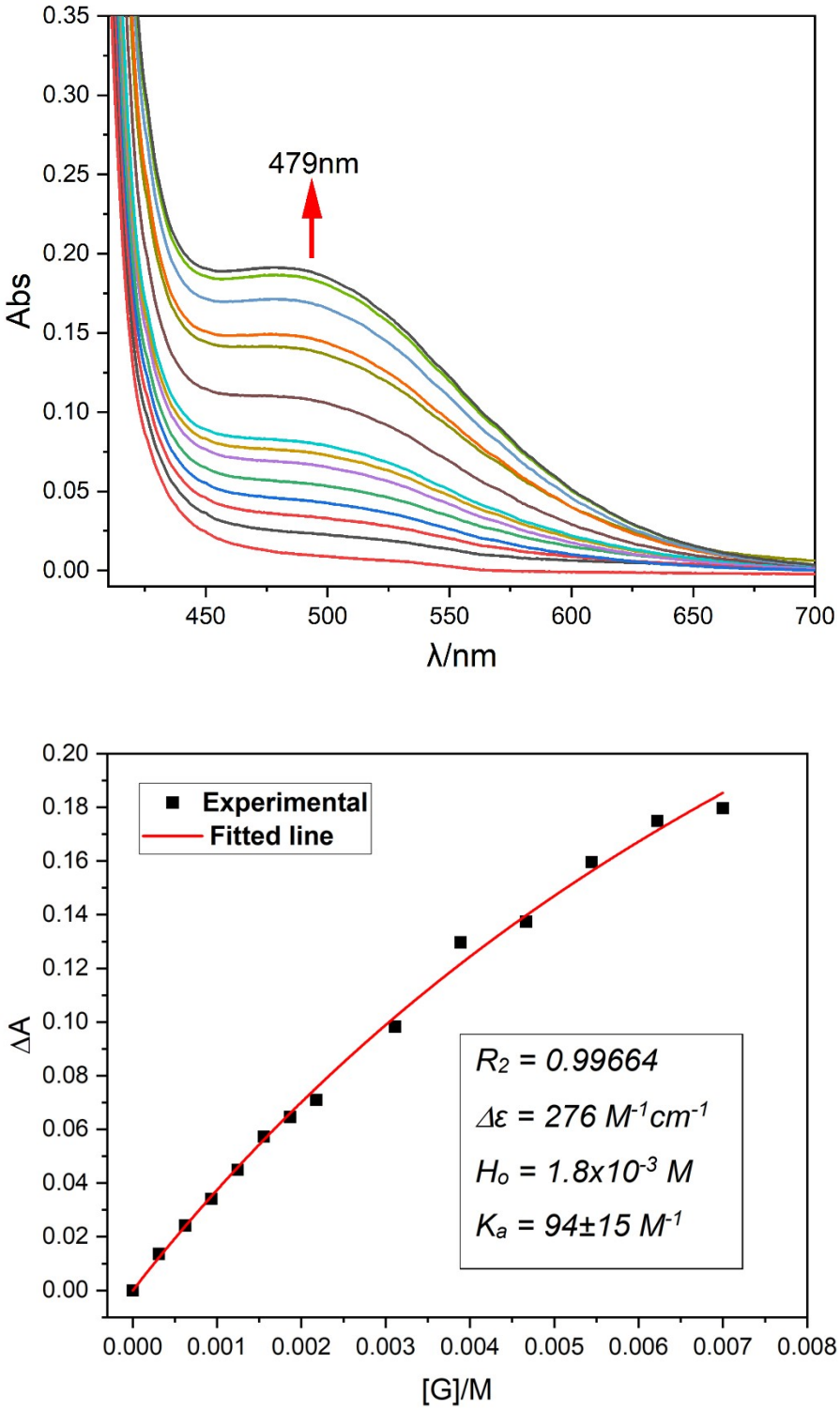

Fig. S29. Top: stacked UV-Vis spectra obtained by titrating **G3** into a mixed H_2O/DMSO solution (9:1, v/v) of **TBox-5**·2Cl (1.8×10^{-3} M) at 298 K. The mixed solution was used because of the low solubility of **G3** in pure water. Bottom: the nonlinear curve-fitting for the complexation of **TBox-5**$^{2+}$ with **G3** to give an association constant of 94 ± 15 M^{-1}.

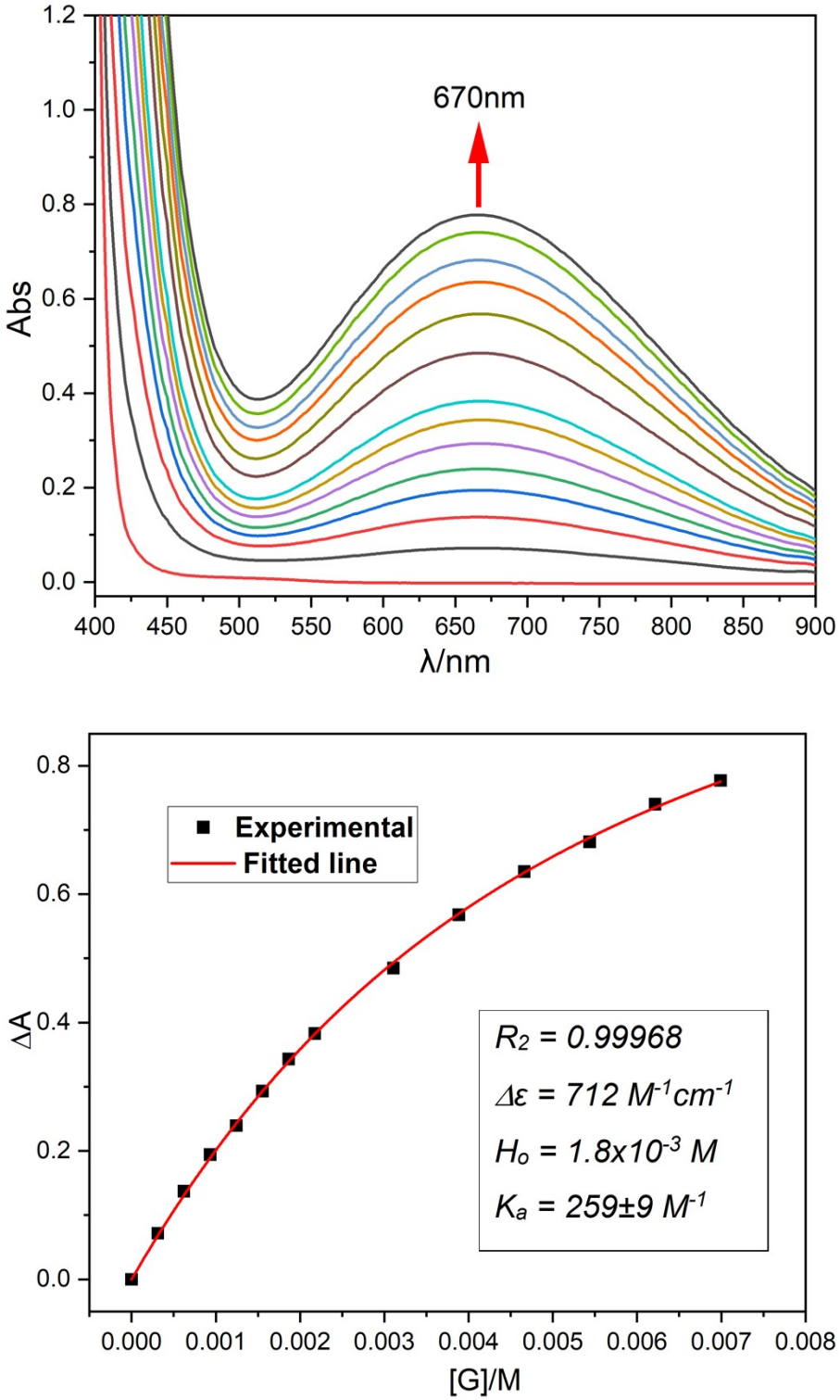

Fig. S30. Top: stacked UV-Vis spectra obtained by titrating **G4** into a mixed H_2O/DMSO solution (9:1, v/v) of **TBox-5**·2Cl (1.8×10^{-3} M) at 298 K. The mixed solution was used because of the low solubility of **G4** in pure water. Bottom: the nonlinear curve-fitting for the complexation of **TBox-5**$^{2+}$ with **G4** to give an association constant of 259 ± 9 M^{-1}.

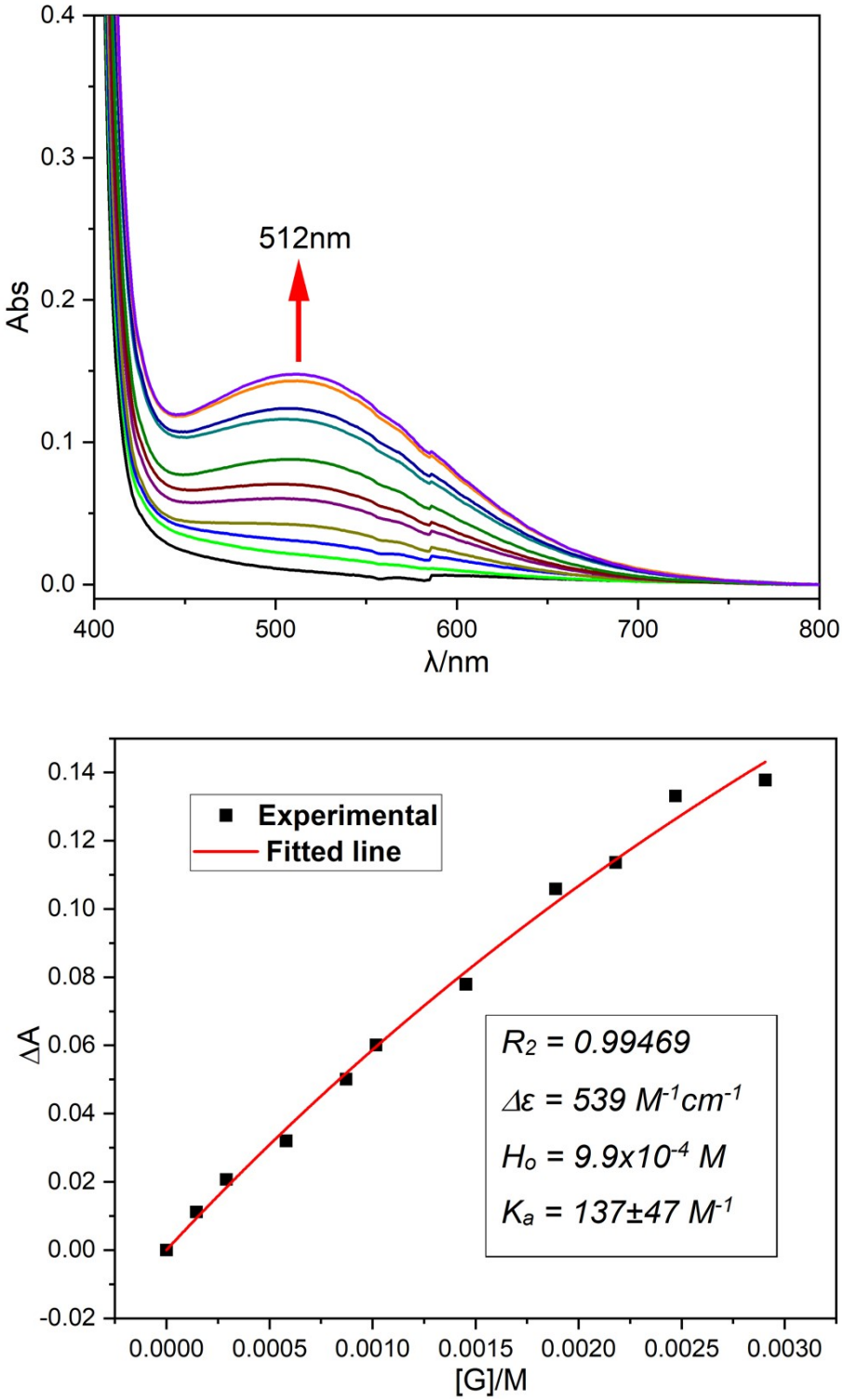

Fig. S31. Top: stacked UV-Vis spectra obtained by titrating **G5** into a mixed H_2O/DMSO solution (5:1, v/v) of **TBox-5**·2Cl (9.9×10^{-4} M) at 298 K. The mixed solution was used because of the low solubility of **G5** in pure water. Bottom: the nonlinear curve-fitting for the complexation of **TBox-5**$^{2+}$ with **G5** to give an association constant of 137 ± 47 M^{-1}.

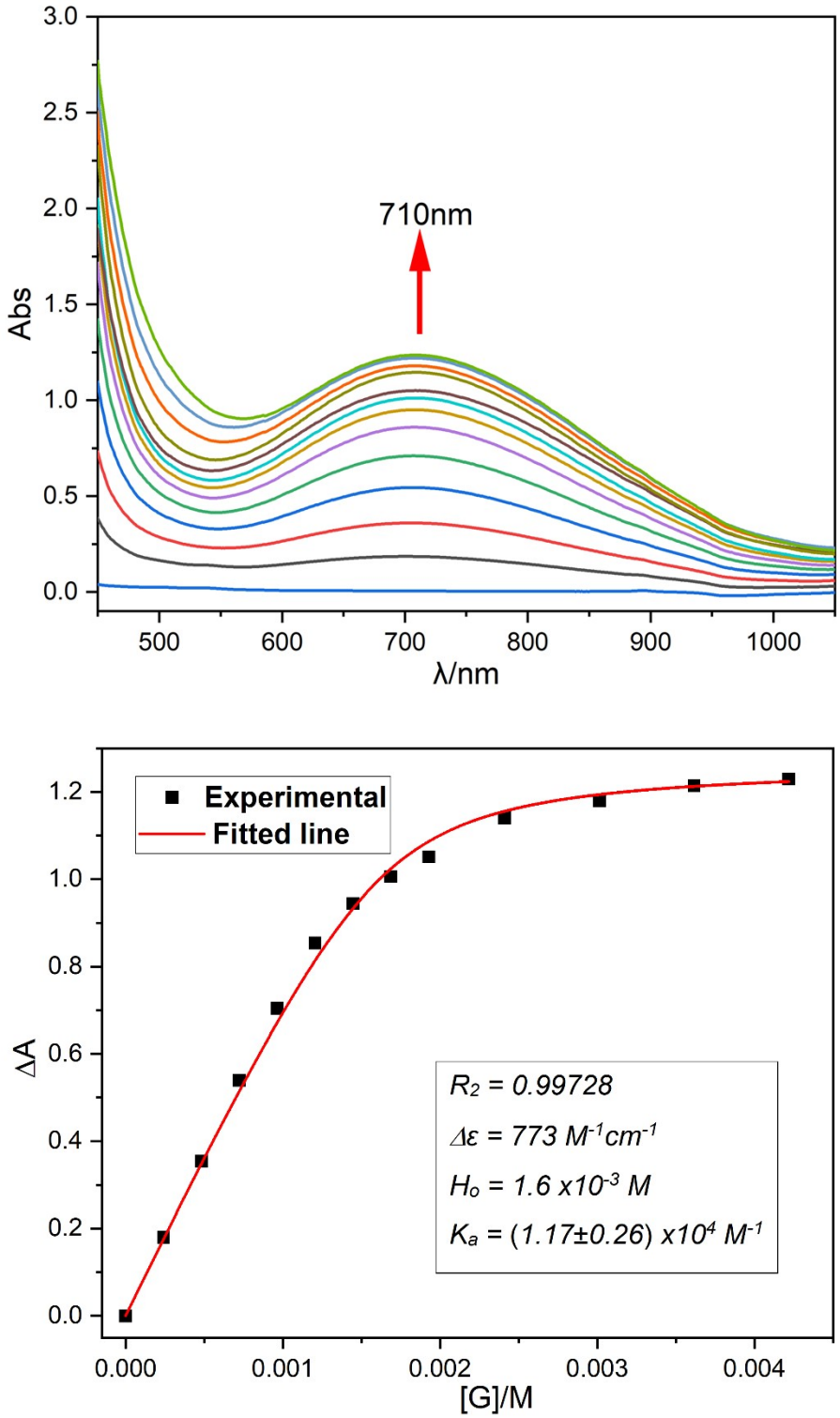

Fig. S32. Top: stacked UV-Vis spectra obtained by titrating **G6** into a mixed H_2O/DMSO solution (6.6:1, v/v) of **TBox-6**·2Cl (1.6×10^{-3} M) at 298 K. The mixed solution was used because of the low solubility of **G6** in pure water. Bottom: the nonlinear curve-fitting for the complexation of **TBox-6**$^{2+}$ with **G6** to give an association constant of $(1.17 \pm 0.26) \times 10^4$ M^{-1}.

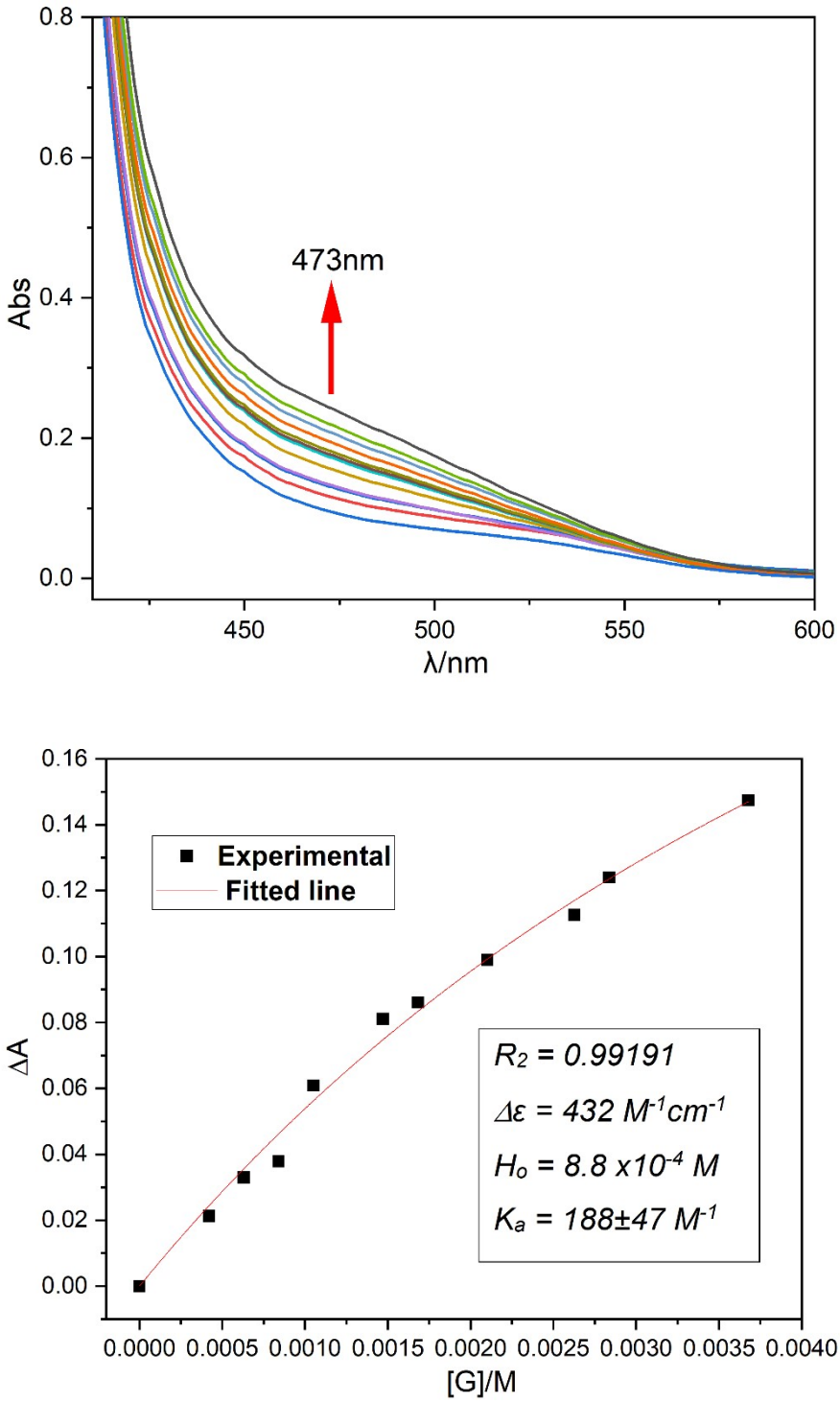

Fig. S33. Top: stacked UV-Vis spectra obtained by titrating **G7** into a mixed H_2O/DMSO solution (11:1, v/v) of **TBox-6**·2Cl (8.8×10^{-4} M) at 298 K. The mixed solution was used because of the low solubility of **G7** in pure water. Bottom: the nonlinear curve-fitting for the complexation of **TBox-6**$^{2+}$ with **G7** to give an association constant of 188 ± 47 M^{-1}.

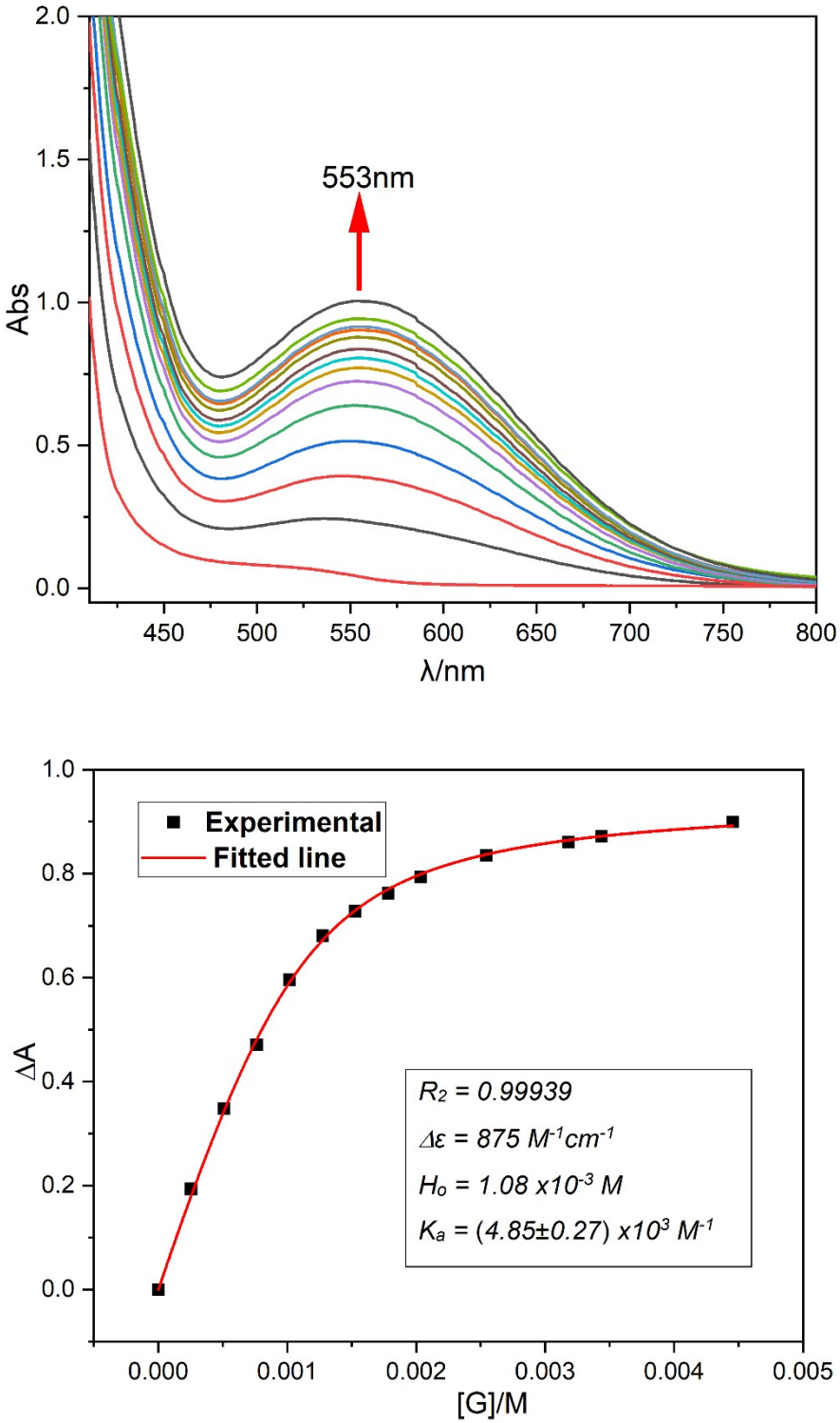

Fig. S34. Top: stacked UV-Vis spectra obtained by titrating **G8** into a mixed H_2O/DMSO solution (2.5:1, v/v) of **TBox-6**·2Cl (1.08×10^{-3} M) at 298 K. The mixed solution was used because of the low solubility of **G8** in pure water. Bottom: the nonlinear curve-fitting for the complexation of **TBox-6**$^{2+}$ with **G8** to give an association constant of $(4.85 \pm 0.27) \times 10^3$ M^{-1}.

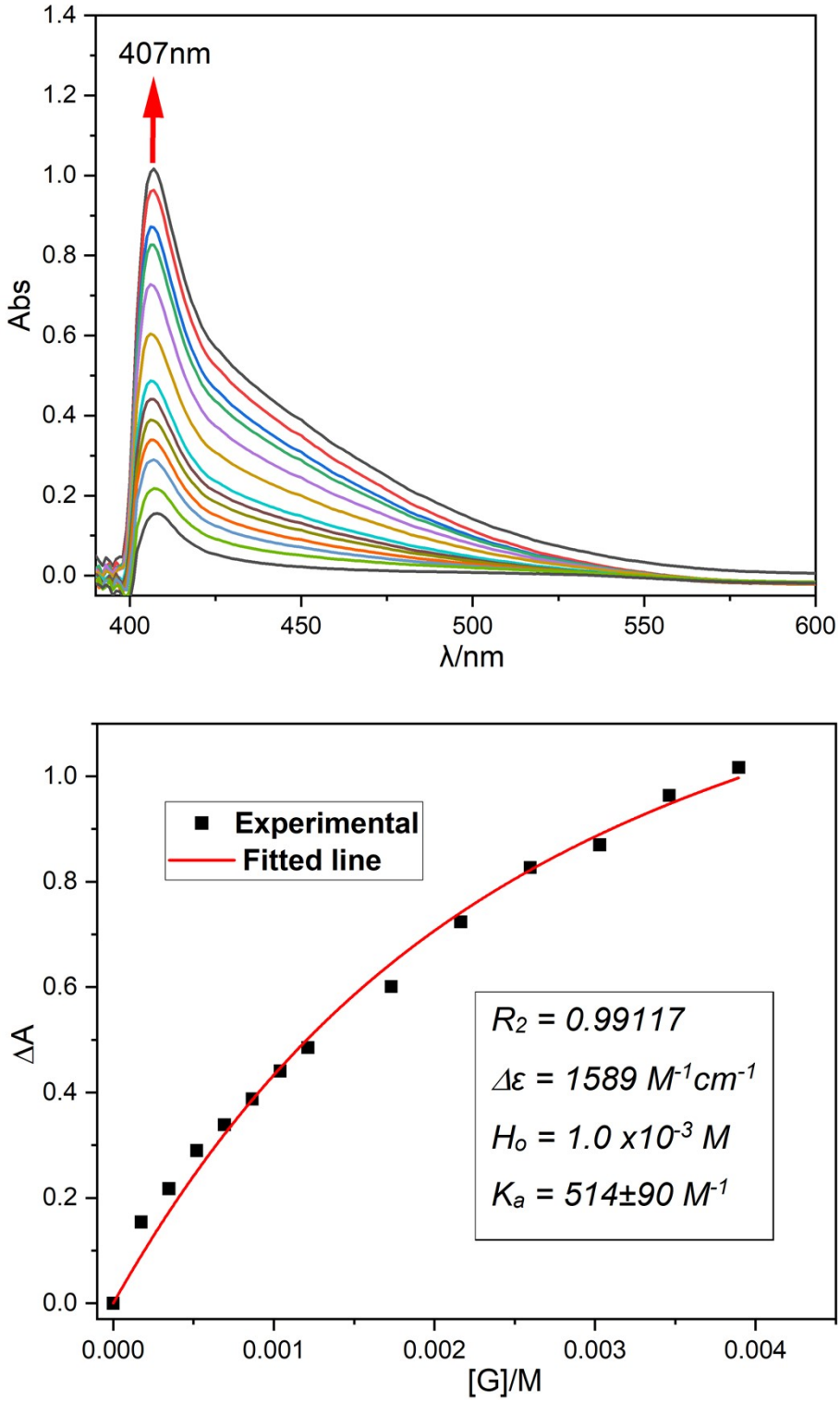

Fig. S35. Top: stacked UV-Vis spectra obtained by titrating **G9** into a mixed H_2O/DMSO solution (1:1, v/v) of **TBox-6**·2Cl (1.0×10^{-3} mol/L) at 298 K. For clarity of absorption bands of host-guest complex at 407 nm, the absorption of host **TBox-6**$^{2+}$ has been subtracted. Bottom: the nonlinear curve-fitting for the complexation of **TBox-6**$^{2+}$ with **G9** to give an association constant of 514 ± 90 M^{-1}.

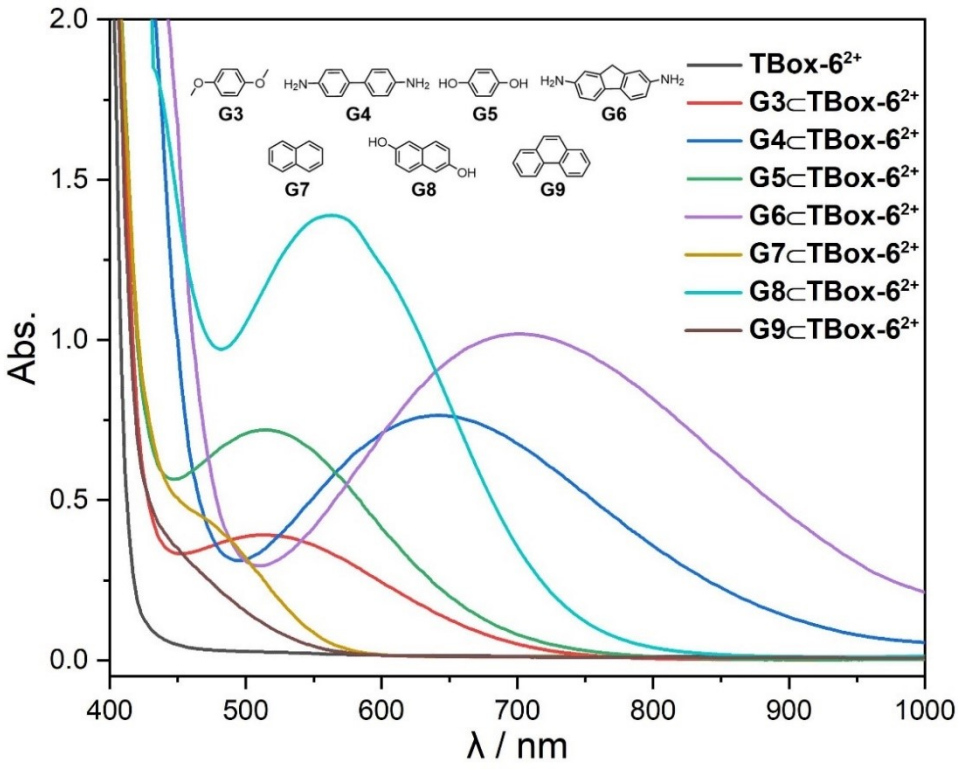

Fig. S36. UV-Vis spectra obtained by adding **G3-G9** into aqueous solution of **TBox-6**$^{2+}$ (1.7×10^{-3} M) at 298 K.

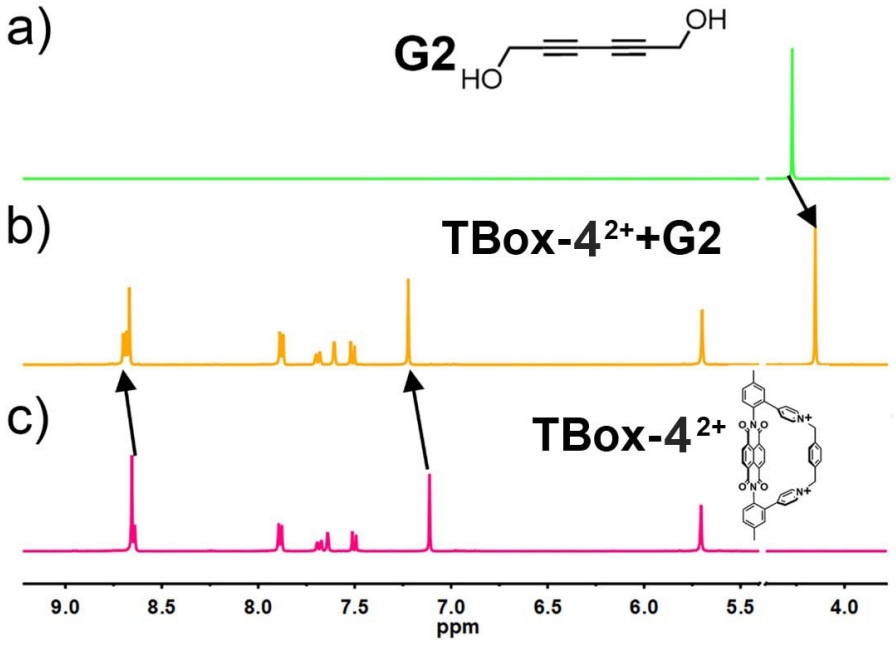

Fig. S37. ^{1}H NMR spectra (600 MHz, D_2O, 298 K) of a) G2, c) TBox-4^{2+}, and b) their mixture. These spectra verify the formation of the host-guest complex between **G2** and **TBox-4**$^{2+}$.

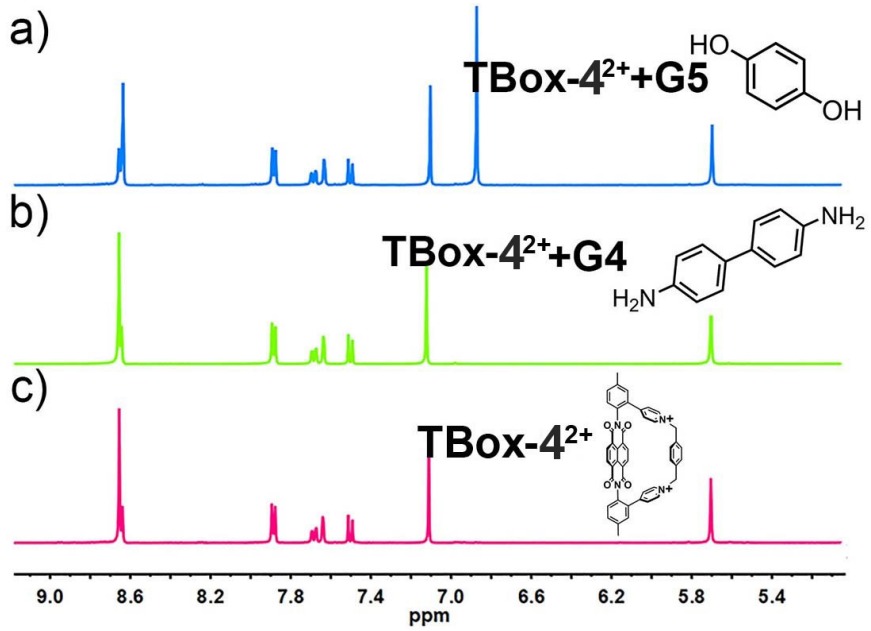

Fig. S38. ^{1}H NMR spectra (600 MHz, D_2O, 298 K) of a) **G5** + **TBox-4**$^{2+}$, b) **G4** + **TBox-4**$^{2+}$, and c) **TBox-4**$^{2+}$. These spectra indicate **G4-G5** cannot be encapsulated into the internal cavity of **TBox-4**$^{2+}$ in water.

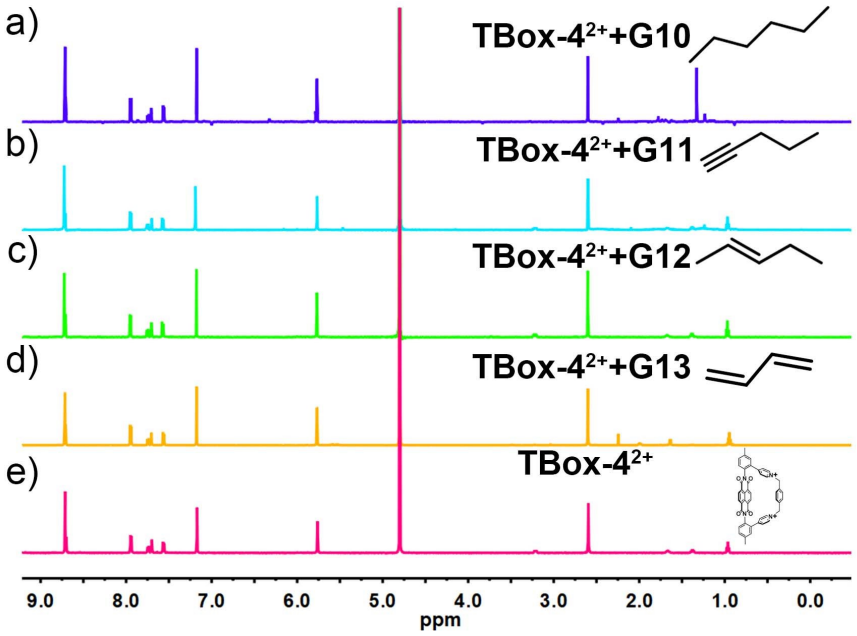

Fig. S39. ^{1}H NMR spectra (600 MHz, D_2O, 298 K) of a) **G10** + **TBox-4**$^{2+}$, b) **G11** + **TBox-4**$^{2+}$, c) **G12** + **TBox-4**$^{2+}$, d) **G13** + **TBox-4**$^{2+}$ and e) **TBox-4**$^{2+}$. These spectra indicate **G10-G13** cannot be encapsulated into the internal cavity of **TBox-4**$^{2+}$ in water.

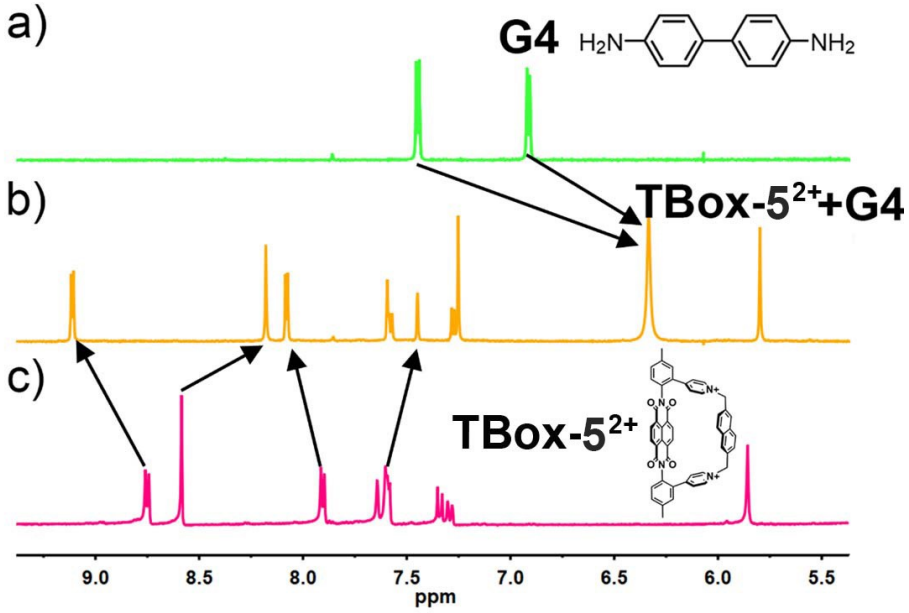

Fig. S40. ^{1}H NMR spectra (600 MHz, D_2O, 298 K) of a) **G4**, c) **TBox-5^{2+}**, and b) their equimolar mixture. These spectra verify the formation of the host-guest complex between **G4** and **TBox-5^{2+}**.

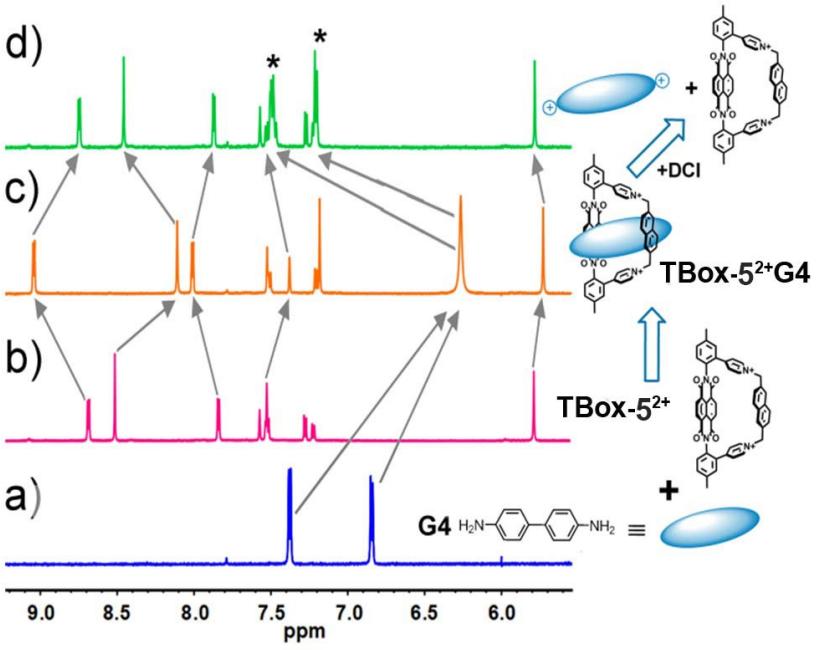

Fig. S41. Partial ^{1}H NMR spectra in D_2O of (a) **G4**, (b) **TBox-5^{2+}**, (c) equimolar mixture of **TBox-5^{2+}/G4** and d) adding deuterated hydrochloric acid to the mixture of **TBox-5^{2+}/G4** (asterisks indicate the proton signals of protonated **G4**).

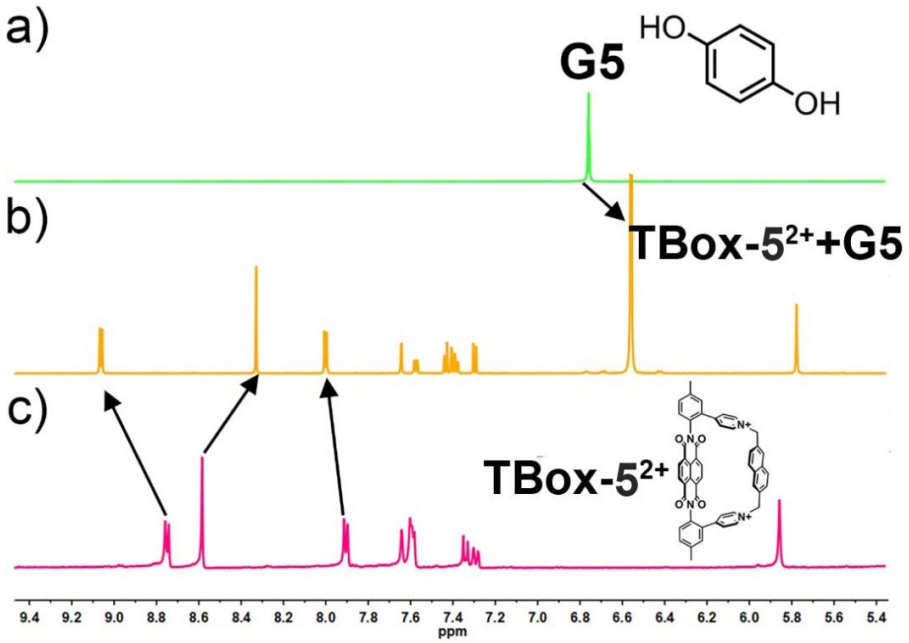

Fig. S42. ^{1}H NMR spectra (600 MHz, D_2O, 298 K) of a) **G5**, c) **TBox-5**$^{2+}$, and b) their equimolar mixture. These spectra verify the formation of the host-guest complex between **G5** and **TBox-5**$^{2+}$.

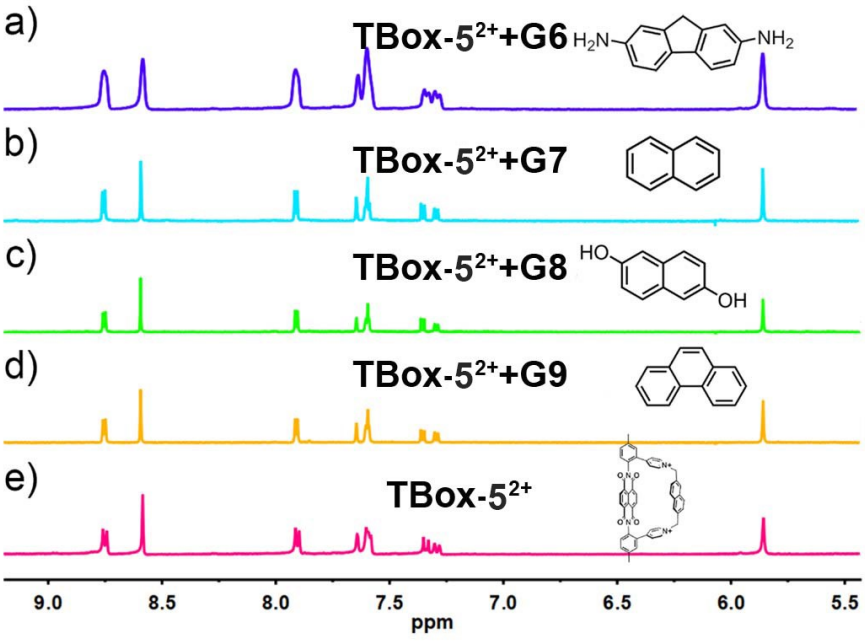

Fig. S43. ^{1}H NMR spectra (600 MHz, D_2O, 298 K) of a) **G6** + **TBox-5**$^{2+}$, b) **G7** + **TBox-5**$^{2+}$, c) **G8** + **TBox-5**$^{2+}$, d) **G9** + **TBox-5**$^{2+}$ and e) **TBox-5**$^{2+}$. These spectra indicate that **G6-G9** cannot be encapsulated into the internal cavity of **TBox-5**$^{2+}$ in water.

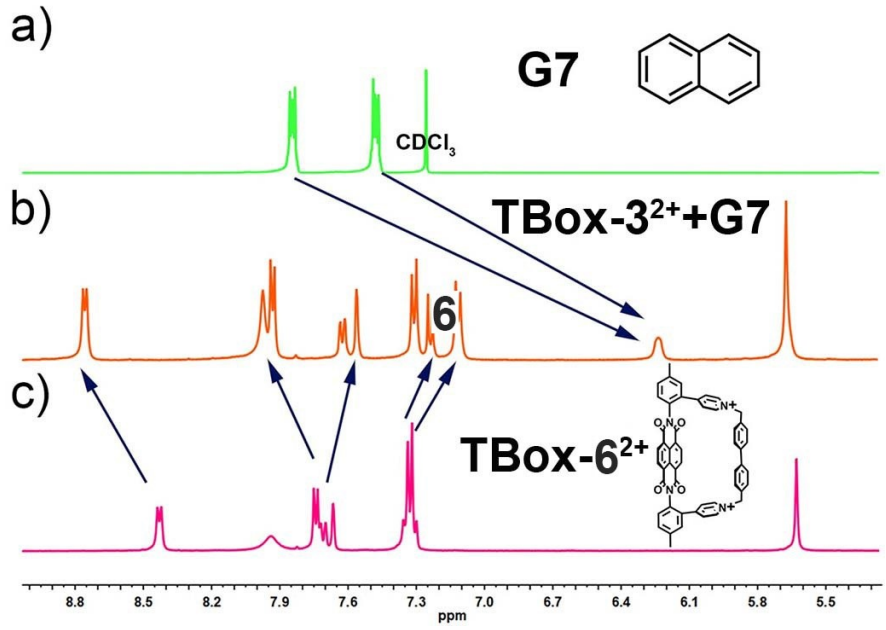

Fig. S44. ^{1}H NMR spectra of a) **G7** in $CDCl_3$, b) **G7**+**TBox-6**$^{2+}$ in D_2O and c) **TBox-6**$^{2+}$ in D_2O. These spectra verify the formation of the host-guest complex between **G7** and **TBox-6**$^{2+}$.

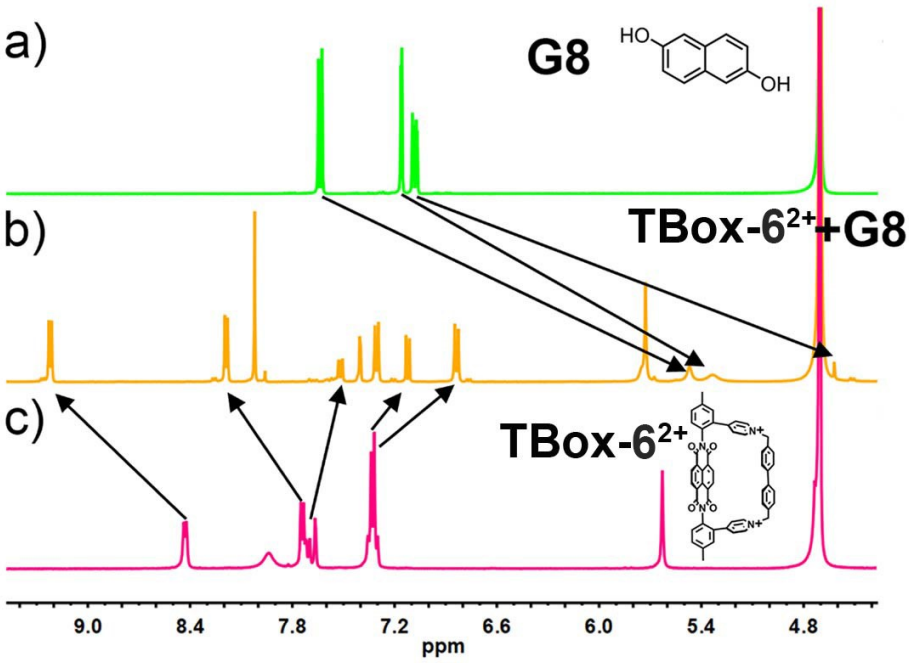

Fig. S45. ^{1}H NMR spectra (600 MHz, D_2O, 298 K) of a) **G8**, b) **G8** + **TBox-6**$^{2+}$ and c) **TBox-6**$^{2+}$**.** These spectra verify the formation of the host-guest complex between **G8** and **TBox-6**$^{2+}$.

6. Near-infrared photothermal conversion

The preparation of charge-transfer complex G6⊂TBox-6^{2+}: To **TBox-6^{2+}** (2.0 mL, 2 mM) solution, 2,7-diaminofluorene (1.5 mg) was added, then the mixture was sonicated about 30 min. After that, the green solution (**G6⊂TBox-6^{2+}**) was collected by vacuum filtration.

Photothermal conversion experiments: The solution of **G6⊂TBox-6^{2+}** (1.0 mL, 2 mM) was irradiated by 808 nm laser (1.0 W/cm^2) in a quartz cuvette. The variation of temperature was recorded by FOTRIC 326C camera. Similar experiments were also carried out for pure water as the blank control.

Calculation of photothermal conversion efficiency: The conversion efficiency was determined according to the previous method.[S8,S9] The photothermal conversion efficiency (η) of **G6⊂TBox-6^{2+}** was calculated by monitoring temperature change of **G6⊂TBox-6^{2+}** in aqueous (2 mM) as a function of time under continuous laser irradiation (808 nm, 1 W/cm^2) for 10 min (t). η was determined according to Equation (a):

$$\eta = \frac{hS(T_{max} - T_{surr}) - Q_{dis}}{I\left(1 - 10^{-A_{808}}\right)} \qquad \text{(a)}$$

where h is heat transfer coefficient, S is the surface area of the container, T_{max} is the maximum system temperature (57.1 °C), and T_{surr} is ambient temperature of the surroundings (25.1 °C). Q_{dis} represents the heat dissipation from the light absorbed by the solvent and the quartz sample cell, I is the incident laser power (1 W/cm^2), and A_{808} is the absorbance of the sample at 808 nm (0.8664). The value of hS is obtained from Equation (b):

$$\tau_s = \frac{m_D c_D}{hS} \qquad \text{(b)}$$

where, m_D and c_D represent the mass (1.0 g) and heat capacity (4.2 J/g), respectively. τ_s is the time constant for heat transfer of the system, which is calculated from Equation (c):

$$t = -\tau_s \ln(\theta) = -\tau_s \ln\left(\frac{T - T_{surr}}{T_{max} - T_{surr}}\right) \qquad \text{(c)}$$

where, t is the cooling time points after continuous irradiation for 10 mins, T is the corresponding temperature of **G6⊂TBox-6^{2+}** during the cooling stage, and according to Fig. S43, τ_s is calculated to be 258 s. Based on Equation (b) and (c), the value of hS is determined to be 0.0163 W. Q_{dis}

represents the heat dissipation from the light absorbed by the water and the container, which is determined according to Equation (d):

$$Q_{dis} = \frac{m_D c_D (T_{mas(water)} - T_{surr})}{\tau_{s(water)}} \quad \text{(d)}$$

Where, $T_{max\ (water)}$ is 26.6 °C and τ_{water} is 243 s, thus Q_{dis} was determined to be 0.0259 W. According to the experiment data and Equation (a), η was calculated to be 57.4 %.

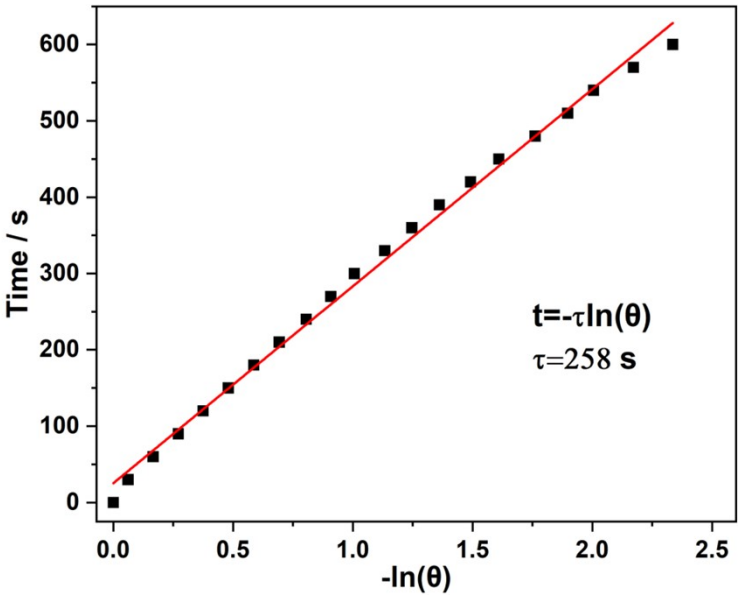

Fig. S46. The Plot of time versus -ln(θ) of **G6⊂TBox-6**$^{2+}$.

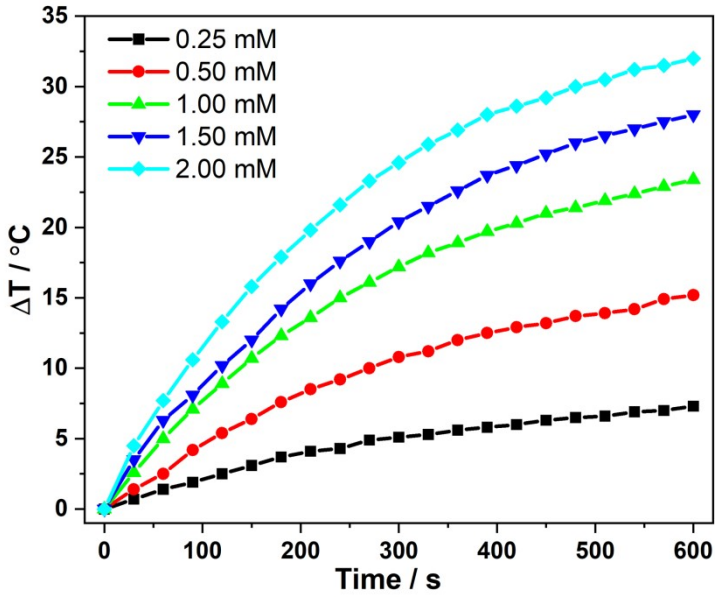

Fig. S47. Heating curves of **G6⊂TBox-6**$^{2+}$ under 808 nm laser (1.0 W cm^{-2}) irradiation of different concentrations.

7. Photothermal Antibacterial Results

Preparation of bacterial solutions: A single colony of *E. coli* on a solid Luria-Bertani (LB) agar plate was transferred to 15 mL of liquid LB culture medium and was grown at 37 °C for 6 h. Then bacteria were washed with PBS, centrifugated (5000 rpm, 3 min) for 3 times, and resuspended in PBS at OD_{600} of ~ 1.2.

Antibacterial activity Assessment of G6⊂TBox-6^{2+}: 50 μL of *E. coli* suspension (OD_{600} ≈ 1.2) was incubated with 250 μL **G6⊂TBox-6^{2+}** solution (0.48 mM) for 5 min. Then, two sets of the *E. coli* suspensions which have been treated with **G6⊂TBox-6^{2+}** solution were kept in the dark or irradiated by a 808 nm NIR laser from 2.5 to 15 min. Finally, all of the *E. coli* suspensions were serially diluted 1 × 10^5 fold with PBS. A 100 μL portion of the dilution with bacteria was spread on the solid LB agar plate, and the colonies formed after 14-16 h incubation at 37 °C were counted. All the experiments were performed in triplicate. The live bacteria ratio was determined by calculating the number of colony-forming units (CFU). The CFU ratio was calculated according to the following equation (e):

$$CFU\ Ratio = \frac{C}{C_0} \times 100\% \qquad \text{(e)}$$

C is the CFU of the experimental group treated with **G6⊂TBox-6^{2+}** under NIR irradiation, and C_0 is the CFU of the control group without any treatments (**G6⊂TBox-6^{2+}** and NIR irradiation).

For non-specific antibacterial behavior of **G6⊂TBox-6^{2+}**, 50 μL of *E. coli* suspensions (OD_{600} ≈ 1.2) were incubated with 250 μL PBS as control group or with 250 μL 0.48 mM **G6⊂TBox-6^{2+}** solution as experimental group (to form 0.40 mM solution) in dark for 15 min. The *E. coli* suspensions were serially diluted 1 × 10^5 fold with PBS, spread on the solid LB agar plate, and the formed colonies after incubation at 37 °C were then counted. The result showed that the bacterial viability ratio is 81.5% after the treatment of **G6⊂TBox-6^{2+}** (0.40 mM).

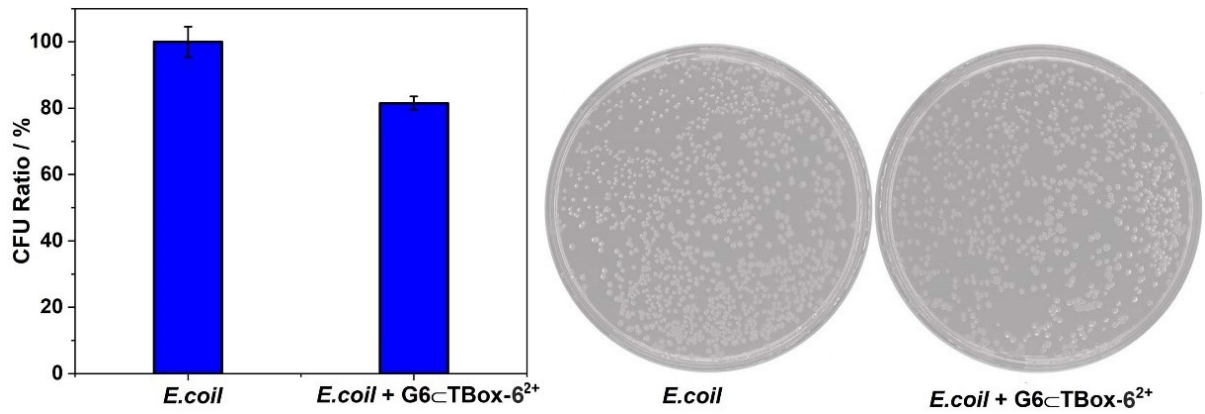

Fig. S48. The non-specific antibacterial behavior of **G6⊂TBox-6^{2+}** (0.40 mM).

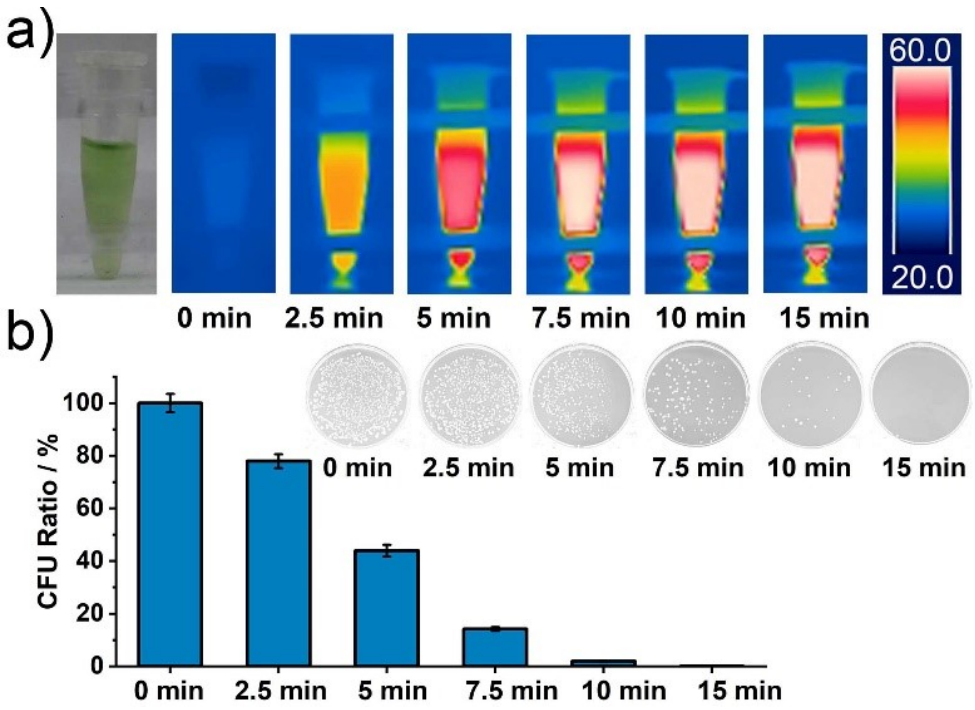

Fig. S49. a) Infrared thermal images of **G6⊂TBox-6^{2+}** (0.4 mM) in the presence of *B.subtilis* under 808 nm irradiation at 1.0 W cm^{-2} for different times. b) CFU for *B.subtilis* treated with **G6⊂TBox-6^{2+}** under the same irradiation conditions as a), and error bars represent standard deviation, N = 3; inset: plate coating results.

8. References

[S1] G. M. Sheldrick, SADABS: Program for Empirical Absorption Correction of Area Detector Data; University of Göttingen, Göttingen, Germany, 1996.

[S2] G. M. Sheldrick, SHELXL-97, Program for Solution of Crystal Structures, University of Göttingen, Göttingen, Germany, 1997.

[S3]. Gaussian 09, Revision A.02, M. J. Frisch, G. W. Trucks, H. B. Schlegel, G. E. Scuseria, M. A. Robb, J. R. Cheeseman, G. Scalmani, V. Barone, G. A. Petersson, H. Nakatsuji, X. Li, M. Caricato, A. Marenich, J. Bloino, B. G. Janesko, R. Gomperts, B. Mennucci, H. P. Hratchian, J. V. Ortiz, A. F. Izmaylov, J. L. Sonnenberg, D. Williams-Young, F. Ding, F. Lipparini, F. Egidi, J. Goings, B. Peng, A. Petrone, T. Henderson, D. Ranasinghe, V. G. Zakrzewski, J. Gao, N. Rega, G. Zheng, W. Liang, M. Hada, M. Ehara, K. Toyota, R. Fukuda, J. Hasegawa, M. Ishida, T. Nakajima, Y. Honda, O. Kitao, H. Nakai, T. Vreven, K. Throssell, J. A. Montgomery, Jr., J. E. Peralta, F. Ogliaro, M. Bearpark, J. J. Heyd, E. Brothers, K. N. Kudin, V. N. Staroverov, T. Keith, R. Kobayashi, J. Normand, K. Raghavachari, A. Rendell, J. C. Burant, S. S. Iyengar, J. Tomasi, M. Cossi, J. M. Millam, M. Klene, C. Adamo, R. Cammi, J. W. Ochterski, R. L. Martin, K. Morokuma, O. Farkas, J. B. Foresman, and D. J. Fox, Gaussian, Inc., Wallingford CT, 2016.

[S4]. M. Cossi, N. Rega, G. Scalmani and V. Barone, *J. Comput. Chem*., 2003, **24**, 669-681.

[S5]. P. J. Stephens, F. J. Devlin, C. F. Chabalowski and M. J. Frisch, *J. Phys.Chem*., 1994, **98**, 11623-11627.

[S6]. S. Grimme, J. Antony, S. Ehrlich and H. Krieg, *J. Chem. Phys*., 2010, **132**, 154104.

[S7] H. Cong, L.-L. Tao, Y.-H. Yu, Z. Tao, F. Yang, Y.-J. Zhao, S.-F. Xue, G. A. Lawrance and G. Wei, *J. Phys. Chem. A.,* 2007, **111**, 2715-2721.

[S8] S. Tian, H. Bai, S. Li, Y. Xiao, X. Cui, X. Li, J. Tan, Z. Huang, D. Shen, W. Liu, P. Wang, B. Z. Tang and C. S. Lee, *Angew. Chem., Int. Ed.*, 2021, **60**, 11758-11762

[S9] X. Li, L. Liu, S. Li, Y. Wan, J. X. Chen, S. Tian, Z. Huang, Y. F. Xiao, X. Cui, C. Xiang, Q. Tan, X. H. Zhang, W. Guo, X. J. Liang and C. S. Lee, *ACS Nano*., 2019,**13**, 12901-12911.